INFORMATION TO USERS

This material was produced from a microfilm copy of the original document. While the most advanced technological means to photograph and reproduce this document have been used, the quality is heavily dependent upon the quality of the original submitted.

The following explanation of techniques is provided to help you understand markings or patterns which may appear on this reproduction.

1. The sign or "target" for pages apparently lacking from the document photographed is "Missing Page(s)". If it was possible to obtain the missing page(s) or section, they are spliced into the film along with adjacent pages. This may have necessitated cutting thru an image and duplicating adjacent pages to insure you complete continuity.

2. When an image on the film is obliterated with a large round black mark, it is an indication that the photographer suspected that the copy may have moved during exposure and thus cause a blurred image. You will find a good image of the page in the adjacent frame.

3. When a map, drawing or chart, etc., was part of the material being photographed the photographer followed a definite method in "sectioning" the material. It is customary to begin photoing at the upper left hand corner of a large sheet and to continue photoing from left to right in equal sections with a small overlap. If necessary, sectioning is continued again — beginning below the first row and continuing on until complete.

4. The majority of users indicate that the textual content is of greatest value, however, a somewhat higher quality reproduction could be made from "photographs" if essential to the understanding of the dissertation. Silver prints of "photographs" may be ordered at additional charge by writing the Order Department, giving the catalog number, title, author and specific pages you wish reproduced.

5. PLEASE NOTE: Some pages may have indistinct print. Filmed as received.

University Microfilms International
300 North Zeeb Road
Ann Arbor, Michigan 48106 USA
St. John's Road, Tyler's Green
High Wycombe, Bucks, England HP10 8HR

LASER INDUCED VIBRATIONAL ENERGY TRANSFER AND CHEMICAL REACTIONS

by

SHIANN-TSAI LIN

A dissertation submitted to the Graduate Faculty in Chemistry in partial fulfillment of the requirements for the degree of Doctor of Philosophy, The City University of New York

1977

This manuscript has been read and accepted for the Graduate Faculty in Chemistry in satisfaction of the dissertation requirement for the degree of Doctor of Philosophy.

February 14, 1978
date

A. M. [signature]
Chairman of Examining Committee

2/15/78
date

Leonard H. Schwartz
Executive Officer

Raymond L. Disch
[signature]
[signature]
Supervisory Committee

The City University of New York

Abstract

LASER INDUCED VIBRATIONAL ENERGY TRANSFER AND CHEMICAL REACTIONS

by

SHIANN-TSAI LIN

Adviser: Professor Avigdor M. Ronn

Fluorescence risetimes and falltime have been studied in ~5μ and >14μ regions after ν_2 mode of CD_3Br is excited by a Q-switched CO_2 laser. Around 5μ, activation occurs in approximately 10 gas kinetic collisions and in the region beyond 14μ, activation requires 77 collisions. Deactivation of both signals occurs at about the same rate, corresponding to 550 collisions. Mechanisms and comparisons to other systems are discussed in terms of energy gaps and breathing sphere parameters for the processes involved.

Laser-induced isotope separation in SF_6 and SF_6 mixtures, reactions of SF_6 and CH_2F_2 and a series of fluoromethanes have been studied by a simple, inexpensive pulsed TEA CO_2 laser. This laser has output energy of ~3J and a pulse duration of 300 ns FWHM and a 700 ns tail.

Experimental results with SF_6 rare-gas mixtures point out the importance of collision-induced dissociation following the initial collisionless dissociation. Rotational relaxation induced by rare gases and H_2 is shown to play a significant role in the dissociation of both isotopic species. Total vibrational relaxation (V-T/R) induced by

H_2 as a collision partner is shown to dominate the dissociation efficiency of SF_6/H_2 mixtures.

Particle formation is observed during a laser pulse in the reaction of SF_6 and SF_6 mixtures. In the absence of H_2, no particulates are found due to rapid recombination, while with H_2, two different sizes of particulates are observed depending on the available produced sulfur. A higher initial pressure of SF_6 results in larger size particulates, a rough measurement on the size of the particulates with a 50/50 mixture is 2 μm.

Reactions of CH_2F_2 excited in its C-F stretching mode show evidence of CF_2 radical involvement in the neat gas. Reactions with molecular chlorine display at least two distinct mechanisms at different pressure regimes. Comparisons are made with other unimolecular dissociations and bimolecular reactions induced by multiphoton absorption from similar laser sources. Product formation of reactions with molecular oxygen shows a dependence on the cell sizes and a non-thermal explosion is ignited at a 1:1 ratio with a threshold pressure of 20 torr.

Threshold pressures of fluoromethanes are determined by irradiation with a non-resonant laser light at identical laser conditions. Threshold pressures are found to be proportional to the ionization potentials of molecules in this series. Product formations of all four species show that the characteristics of the reactions agree well with a model based on short reaction time, high temperature and rapid, automatic quenching.

ACKNOWLEDGMENTS

I would like to express my gratitude to Professor Avigdor M. Ronn, my research advisor, for his stimulating direction, readily available consultation and financial help. I am indebted to Dr. Boyd L. Earl for his help in my early research days. I am deeply grateful to Dr. Shu M. Lee for his constant readiness to help in any way he could. To Ronn's group, especially Barbara Fauls, Jaime Nieman and Alan Schwebel, I would also like to express my indebtedness for their friendship and interesting discussions. I am grateful to Professor Takanobu Ishida for supplying the CHF_3 and CF_4 samples. Thanks to Professor Jose Riveros for his helpful advice and literature information.

I thank my family and friends for their encouragement. Special thanks to my wife for her sacrifice throughout my college years and for her typing of this dissertation.

Table of Contents

List of Tables

List of Figures

Chapter 1

INTRODUCTION

Since the initial demonstration of laser[1] operation using ruby in 1960[2], lasing action has been achieved in gases, liquids and solids at wavelengths ranging from the far infrared to the ultraviolet region of the spectrum. Undoubtedly, the most important gas laser from both an industrial and scientific point of view is the CO_2 laser[3,4], in which transitions between vibrational-rotational levels can provide large continuous-wave or pulsed power, with relatively high efficiency (up to 30 percent) at numerous discrete wavelengths separated from each other by about 2 cm^{-1} in the region from 920 to 1090 cm^{-1}. The fact that many molecules show absorption features in this region, together with the discovery that chemical reactions can be selectively activated with monochromatic and high intensity infrared radiation[5], has led to the widespread use of the CO_2 laser.

The monochromatic nature of the laser radiation guarantees that only the molecular species which have the particular energy levels matching the laser's frequency can be excited. Therefore, following the absorption of the laser radiation the energy transfer among the vibrational, rotational and translational degrees of freedom can be studied by monitoring the intensity of fluorescence, which depends linearly on the number of molecules in particular vibrational states. The processes of the collisional activation and deactivation at a particular vibrational mode, in general, are assumed as the following:

$$A^*(\nu_i) + A^*(\nu_i) = A^*(2\nu_i) + A + \Delta E$$
$$A^*(\nu_i) + A^*(2\nu_i) = A^*(3\nu_i) + A + \Delta E$$
$$A^*(n\nu_i) + A = A^*(\nu_j) + A + \Delta E$$
$$A^*(\nu_i) + A = A + A + \Delta E$$

where n is an integer. Thus, the activation (V-V) and deactivation (V-T/R) rates can be obtained from the observed fluorescence intensities. The fluorescence signal shows a sudden increase, corresponding to fast vibrational-vibrational (V-V) energy transfer, and then decays exponentially back to its ambient level, corresponding to slow vibrational-translational/rotational (V-T/R) energy transfer. Laser induced energy transfer in CD_3Br is presented in Chapter 2.

Due to the large energy difference between a single IR laser photon and the required activation energy for chemical reactions, absorption of a single laser photon is not sufficient to initiate a chemical reaction. However, the high intensity of laser radiation, which makes the multiphoton absorption (either sequential single photon, multiphoton or both) processes possible, can induce chemical reactions. This high power intensity can be achieved by the use of a simple and inexpensive laboratory quality pulsed TEA (transversely excited atmospheric pressure) laser. Chapter 3 presents the constructional and operational details of this inexpensive research tool.

With CO_2 laser radiation, a reaction can be induced in two different ways, through multiphoton absorption processes or by gas breakdown. There are two existing models for collisionless multiphoton

absorption processes. Both have the same basic scheme but differ in the interpretation of the coherent region which controls the selective excitation of the molecules and the subsequent collisionless dissociation of isotopically labeled species. The application of these processes is limited by the available CO_2 photon frequencies, therefore, only molecules posessing infrared absorption frequencies in a range of 9.2 to 11μ can be excited. On the other hand, threshold pressure, instead of available photon frequency, is the only necessary condition to induce a reaction by the gas breakdown method at available laser powers. Three models were proposed for these mechanisms, Chapter 4 presents a short review of the proposed theoretical models for both methods.

Subsequent to multiphoton absorption processes there are two possibilities that may yield a selective chemical reaction. Firstly, the rate of photodissociation of selectively excited molecules should exceed that of resonance transfer and of thermal excitations[6]. Secondly, there must be an efficient extraction step, which may be magnetic, electrical, optical, thermal, heterogeneous, or chemical, that acts preferentially on the excited species before relaxation, collisional energy transfer or charge transfer can occur[7]. Loss of the selectivity, however, leads to a nonselective thermal reaction. Laser-induced isotope separation (LIS) of SF_6 through multiphoton absorption processes, through which some degree of the selectivity has to be maintained, is discussed in Chapter 5.

Since laser-induced resonant excitation of the particular vibrational degree of freedom results in a nonequilibrium distribution in all degrees of freedom, it is interesting to consider whether a

laser-induced chemical reaction, driven either resonantly or nonresonantly, shows differences in product formation and mechanism from a thermally excited reaction. Thermal excitation of vibrational degrees of freedom forms the basis of unimolecular reaction rate theory. The Rice-Ramsperger-Kassel-Marcus (RRKM) theory, which is a statistical theory, assumes that the vibrational energy of the molecule is subject to rapid statistical redistribution. Experimental evidence shows that energy is rapidly redistributed between all vibrational modes of the molecules involved in time intervals no greater than 10^{-11} sec following excitation[8]. Therefore, laser-induced chemical reactions may show a different product formation from thermal reactions if molecules with sufficient energy accumulated in the particular vibrational degree of freedom undergo chemical change before distribution of energy among all degrees of freedom.

With the intense infrared radiation, which is associated with a very high AC electric field, sample molecules that are transparent to laser frequencies can also be dissociated through the formation of electron avalanche (spark) produced by dielectric breakdown (DB). This nonresonant process, which is nonselective in mode excitation, does, however, show thermodynamically controlled product formation[9]. The spark can also be produced in gases which absorb the laser photons. However, the luminescence is always observed prior to the occurrence of breakdown in this resonant process. The formation of a spark is dependent on overcoming distinct pressure and laser intensity thresholds but the luminescence has no such requirements and can be created, without the formation of a spark, under conditions well below those

required for dielectric breakdown. From previous observation in CCl_2F_2, SiF_4 and NH_3 gases the luminescence was found to consist largely of the molecular spectra of dissociation products, whereas, the spark spectrum was dominated by atomic lines[10]. Thus, comparison of the results obtained from different processes and irradiation times may allow for better theoretical understanding of mechanisms at different processes.

In all experiments on laser induced multiphoton absorption and dielectric breakdown, the primary question naturally arises: how to describe the mechanism responsible for the reaction obsreved? It is a difficult problem with an infrared laser-induced chemical reaction to separate the thermal reaction from the reaction of the vibrationally excited species since the repopulation of vibrational energy levels over all degrees of freedom results in an increase in the reaction rate thermally. Thus, the mechanisms which are believed to be feasible under the prevailing experimental conditions are tested from the product distribution of the reaction, qualitatively rather than quantitatively, with the following considerations. Firstly, the power dependence of the reaction was determined so as to allow a calculation of the total efficiency. This efficiency is established on the basis of product formation. The threshold power intensity to drive a chemical reaction is high, usually, on the order of one hundred million watts per square centimeter. Secondly, the pressure dependence on the excited species was investigated so that the effects of collisional events can be determined. At low pressure, the collisional effects are negligible, thus, the unimolecular reaction through multiphoton absorption is

dominant. On the other hand, a threshold pressure indicates collisional events are necessary to acquire enough energy to drive a reaction. There also exists a distinct difference of the threshold pressure between on and off resonance irradiation to induce a chemical reaction. The higher threshold pressure needed in the off-resonance irradiation may be due to the fact that more demanding conditions exist for providing the starting electron for observed optical breakdown of gases. Thirdly, the nature of the scavenger was tested in order to find out the change in the mechanistic route of the preferred channel corresponding to the formation of product distribution. Chapters 6 and 7 deal with the infrared laser-induced chemical reactions of SF_6 and CH_2F_2, respectively. In both species all three conditions discussed above were exhaustively tested.

In Chapter 8 a series of reactions of fluoromethanes were studied so as to examine the relation between the threshold pressure and the molecular properties of a series of gases under DB condition. These were compared with the available data on product formation obtained from a jet method for the same series of species.

Reference

1. The word laser is an acronym for Light Amplification by Stimulated Emission of Radiation.
2. T. H. Maiman, Nature 187, 493 (1960).
3. C. K. N. Patel, Phys. Rev. Lett. 12, 588 (1964).
4. A. L. Robinson, Science 193, 1230 (1976).
5. S. W. Mayer, M. A. Kwock, and R. W. F. Gross, Appl. Phys. Lett. 17, 516 (1970).
6. V. S. Letokhov, Science 180, 451 (1973).
7. S. Kimel and S. Speiser, Chem. Rev. 77, 437 (1977).
8. A. M. Ronn, Chem. Phys. Lett. 42, 202 (1976).
9. P. J. Robinson and K. A. Holbrook, Unimolecular Reactions, Wiley-Interscience, New York 1972.
10. N. R. Isenor and M. C. Richardson, Appl. Phys. Lett. 18, 224 (1971).

Chapter 2

LASER INDUCED VIBRATIONAL ENERGY TRANSFER IN CD_3Br

2.1 Introduction

The methyl halides and their deuterated counterparts provide a convenient series for study by the technique of laser induced fluorescence. They all have absorptions of CO_2 laser lines, and the differences among them make for detailed and interesting comparisons. The first and most extensively studied[1-4] of the series is CH_3F. CH_3Cl has also been the subject of several investigations[5-7]. More recently, CH_3Br[8] and CH_3I[9] have been investigated in our laboratory. This series provided interesting insights into collisional transfer of vibrational energy. We have now extended this investigation to the deuterated CD_3X series. As compared to the CH_3X series, this series exhibits significant changes in the energy level structures of the members and in the parameters considered to be important in determining the probability of energy transfer processes. We report here on the CD_3Br investigation.

2.2 Experimental

The experimental apparatus was a Q-switched CO_2 laser fluorescence set-up as shown in Fig. 1[10]. Laser beam parameters are: individual pulse energy, ~2 mJ; pulse full width half maximum, ~700 μs; beam diameter, 0.7 cm. The fluorescence signal was detected through the viewing window

of the sample cell, which was mounted at right angles to the laser beam. The fluorescence signal in a particular wavelength region could be isolated and detected by appropriate detectors using combinations of window materials and interference filters. The intensity of fluorescence, after excitation by a laser pulse, was monitored as a function of time. The signals were pre-amplified and averaged on a waveform eductor, then displayed on an X-Y recorder for analysis.

A capacitance manometer connected directly to the cell was used for pressure measurements in the cell from 1 mtorr to 100 torr. A typical combined leak-outgas rate of the isolated cell was less than 10 mtorr/hr. The research grade rare gases were all obtained from Matheson Gas Products, Inc. The CD_3Br was 98% minimum isotopic purity. The minimum purities of the rare gases were: He, 99.9999%; Ar, 99.9995%; Ne, Kr and Xe, 99.995%. All measurements were performed at room temperature ($22\pm3^{\circ}C$).

The R(10) line of the 10.6μ band of the CO_2 laser was utilized for all measurements on CD_3Br. This line is absorbed by the P(39) line[11] of the ν_2 (methyl sym-deformation) band of CD_3Br. We estimate less than 5% excitation to ν_2 in the direct path of the beam, compared to a thermal population of 0.82%. Fluorescence was detected in two distinct regions. In the region around 5μ, an InSb ($77^{\circ}K$) detector with a matched amplifier was used, either with no filter, in which case the sapphire detector window limited the wavelength domain to $\lesssim 5.5\mu$, or with one of two filters, 4.65-5.13μ or 4-5μ. The response time of the detector and associated electronics was less than 1 μsec. A MgF_2 cell window was used for these measurements.

Fluorescence at wavelengths longer than 14μ was studied using a KBr window, a combination of two filters, a 13μ longpass and a 14-22μ bandpass, to suppress scattered laser radiation, and a Ge:Cu detector cooled to $4^{o}K$. This detector was loaded to 10KΩ , under which condition the response time was about 1 μsec.

2.3 Results

Fig. 2 shows some of the vibrational energy levels[11] of CD_3Br and indicates the relative position of the pumped level, ν_2. For analysis of the rates of the first order processes, the following method was used. At a given pressure, the rate of the rise or fall of the fluorescence signal was obtained as $1/\tau$ from a plot of fluorescence intensity vs. time displayed on the recorder. τ is the relaxation time which is the time required for the signal to decay to 1/e of its initial value. τ is determined as the reciprocal of the slope of a semi-log plot of signal intensity versus time, the linearity of which attests to the single-exponential character of the signal analyzed. The rate constant for the process was then obtained from the slope of a plot of rate vs. pressure. A linear least-squares method was used for obtaining the best slope. For observing the effect of a rare gas on the deactivation rate, the rare gas was added in steps to a constant pressure of CD_3Br.

For measuring the decay time of the 5μ modes the InSb detector was used without a filter. Using the same set-up, the rare gases were also introduced so as to measure their effects on this deactivation rate. For the latter measurements CD_3Br pressure was 1 torr, and rare gas

pressures were varied from 2 torr-80 torr for He, through comparable values of 7 torr-80 torr for Xe. A plot of the deactivation rate of the 5μ modes vs. CD_3Br pressure is shown in Fig. 2. The rate constant, which is the slope of the line calculated by the least squares method, is 12 ± 2 $msec^{-1}torr^{-1}$ for this deactivation. This rate constant, along with the others measured for CD_3Br, is shown in Table 1. Table 1 also shows the number of gas kinetic collisions required for each process and the probability per gas kinetic collision. This presentation has advantages for relative comparison of different species, as it eliminates any difference in collision rates due purely to mass effects.

The fluorescence in the region from 4.56 to 5.13μ includes the ν_1 (methyl sym-stretching), $2\nu_2$ and $2\nu_5$ bands. The ν_4 (methyl asym-stretching) band may also contribute but it is expected to be a very small part of the total amplitude because the filter will transmit only the long-wavelength tail of this band. This risetime in this region is so fast that a large error is easily introduced into the measured rate. The rate constant for activation was measured at 650 ± 150 $msec^{-1}torr^{-1}$ (measured over a pressure range of 0.4-1.0 torr). Risetime measurements were also performed in the 4-5μ region. In this region, ν_1, ν_4, $2\nu_5$ and $2\nu_2$ bands are all included. The contribution of the ν_4 band is probably so small (due to the relatively small intensity of this band[12]) that no new information was expected. The rate constant for activation in this region is 633 ± 150 $msec^{-1}torr^{-1}$, essentially the same as that of the 4.56-5.13μ fluorescence.

The energy levels at wavelengths longer than 14μ are ν_3 (C-Br stretch) and ν_6 (methyl-rock). The measured rate constants for deactiva-

TABLE 1

Measured CD_3Br Rate Constants

Process	Collision Partner	Rate Constant ($msec^{-1}Torr^{-1}$)	Number of Collisions	Probability Per Collisions
5μ deactivation				
	CD_3Br	12 ± 2	550	1.82×10^{-3}
	He	7.4 ± 1.0	1840	5.43×10^{-4}
	Ne	1.2 ± 0.2	6400	1.55×10^{-4}
	Ar	1.1 ± 0.2	6500	1.54×10^{-4}
	Kr	1.0 ± 0.2	5700	1.75×10^{-4}
	Xe	0.7 ± 0.1	9300	1.07×10^{-4}
5μ activation				
	CD_3Br	650 ± 150	10	0.10
ν_3,ν_6 deactivation				
	CD_3Br	9.5 ± 2.5	700	1.43×10^{-3}
ν_3,ν_6 activation				
	CD_3Br	86 ± 15	77	1.30×10^{-2}

tion and activation of these levels are 9.5 ± 2.5 and 86 ± 9 $msec^{-1}torr^{-1}$, respectively. It is expected initially on the basis of the behavior of similar molecules that the deactivation rate constant of these levels should be the same as that for the 5μ levels (see Discussion). The signal in this region was weak and also showed considerable heating effects in measuring the deactivation rate. The measured deactivation processes (V-T/R) directly convert excess vibrational energy into translational and rotational energy, resulting in an elevated translational temperature which is manifested in a base-line displacement in the V-T/R decay curve. Following V-T/R decay, the translational temperature returns to the ambient value by much slower heat transport processes, on the time scale of 10's or 100's of milliseconds. A pressure of 90.3 torr of Xe was added to the CD_3Br for increasing the heat capacity of the system and reducing this heating, but even under these conditions, the heating was not completely eliminated. Given the experimental difficulties in this region, the agreement between the deactivation rate constant measured and that measured for the 5μ states is reasonable. The results of the long-wavelength measurements are shown in Fig. 4.

2.4 Discussion

In a particular wavelength region, the intensity of fluorescence represents the population of molecules in the vibrational energy levels within this region, so the rates of activation and deactivation of the fluorescence correspond to the rates of collisional energy transfer into and out of the levels, respectively.

Upon the irradiation by the CO_2 laser, energy is absorbed into the ν_2 band. This energy is then distributed among all other vibrational modes by means of V-V energy transfer, such as the following.

$$CD_3Br(\nu_i) + CD_3Br(\nu_i) = CD_3Br(2\nu i) + CD_3Br(0) + \Delta E(= 0) \quad (1)$$

$$CD_3Br(\nu_2) + CD_3Br(0) = CD_3Br(\nu_5) + CD_3Br(0) + \Delta E(= -68\ cm^{-1}) \quad (2)$$

$$CD_3Br(2\nu_2) + CD_3Br(0) = CD_3Br(\nu_1) + CD_3Br(0) + \Delta E(= -176\ cm^{-1}) \quad (3a)$$

$$CD_3Br(2\nu_5) + CD_3Br(0) = CD_3Br(\nu_1) + CD_3Br(0) + \Delta E(= -40\ cm^{-1}) \quad (3b)$$

$$CD_3Br(2\nu_2) + CD_3Br(0) = CD_3Br(\nu_4) + CD_3Br(0) + \Delta E(= -314 cm^{-1}) \quad (4a)$$

$$CD_3Br(2\nu_5) + CD_3Br(0) = CD_3Br(\nu_4) + CD_3Br(0) + \Delta E(= -178\ cm^{-1}) \quad (4b)$$

$$CD_3Br(\nu_1) + CD_3Br(0) = CD_3Br(\nu_4) + CD_3Br(0) + \Delta E(= -138\ cm^{-1}) \quad (5)$$

$$CD_3Br(\nu_2) + CD_3Br(0) = CD_3Br(\nu_3) + CD_3Br(0) + \Delta E(= 415 cm^{-1}) \quad (6a)$$

$$CD_3Br(\nu_5) + CD_3Br(0) = CD_3Br(\nu_3) + CD_3Br(0) + \Delta E(= 483\ cm^{-1}) \quad (6b)$$

$$CD_3Br(\nu_2) + CD_3Br(0) = CD_3Br(\nu_6) + CD_3Br(0) + \Delta E(= 277\ cm^{-1}) \quad (7a)$$

$$CD_3Br(\nu_5) + CD_3Br(0) = CD_3Br(\nu_6) + CD_3Br(0) + \Delta E(= 345\ cm^{-1}) \quad (7b)$$

$$CD_3Br(\nu_6) + CD_3Br(0) = CD_3Br(\nu_3) + CD_3Br(0) + \Delta E(= 138\ cm^{-1}) \quad (8)$$

Eq. (1) is the "up-the ladder" transfer within a single mode. Such processes are generally expected to be very rapid, because they are nearly resonant. Eq. (2)-(8) are intermode crossing processes which occur in order to populate all other modes. These processes include multiply-excited modes in intermode crossing processes.

Eventually, the excess vibrational energy is converted into translational and rotational energy, mainly by V-T/R processes such as

$$CD_3Br(\nu_i) + M = CD_3Br(0) + M + \Delta E(= E_i) \quad (9).$$

In this equation, M may represent a CD_3Br molecule in any state, or a molecule of a different species, such as a rare gas atom. The energy deficit here is equal to the energy of the state undergoing deactivation. This value generally dominates in determining the probability of deactivation from a level, so deactivation proceeds via the lowest level(s).

In postulating the mechanisms responsible for the observed results, one attempts to find the most favorable routes for collisional energy transfer. One first seeks a direct route, i.e., one involving a small number of elementary steps such as Eq. (1)-(8). For each step, there are two criteria which are usually given prime consideration. One is the size of the energy deficit, the ΔE value. The probability of energy transfer generally decreases strongly with increasing energy gap. The other criterion is the magnitude of the "breathing sphere parameters" for the normal modes involved. These parameters function as matrix elements in the expression for energy transfer probability in Stretton's modified SSH theory[13]. For CD_3Br, the values are for the six normal modes $\langle A_1^2\rangle$=0.12, $\langle A_2^2\rangle$=0.091, $\langle A_3^2\rangle$=0.035, $\langle A_4^2\rangle$=0.098, $\langle A_5^2\rangle$=0.096, $\langle A_6^2\rangle$=0.13, all in amu^{-1}. These values are based on the normal coordinate analyses of Refs. 14 and 15. The values for all modes except ν_3 lie in the range 0.11 $\pm$ 0.02, while the value for ν_3 is 0.035. This indicates that for hard collisions, energy transfer involving ν_3 is expected to be somewhat less efficient than that involving the other modes. Hard collisions are those in which the steep repulsive portion of the intermolecular potential is sampled. For transfer of amounts of energy $\gtrsim$ KT, such collisions are of primary importance. Soft, or long-range,

collisions, which sample the attractive part of the potential, are effective in bringing about transfer of smaller amounts of energy.

Following initial excitation of ν_2, transfer into ν_5 should occur quite rapidly by Eq. (2). In CH_3Br, ν_2 and ν_5 exhibit identical kinetics even though they are separated by $\sim$140 cm^{-1}. It is deemed probable that some sort of coupling exists between these modes, and, as Fermi coupling is precluded by symmetry, we propose that the modes are Coriolis coupled. If this applies in CD_3Br as well, a more rapid ν_5 activation is to be expected. Up-the-ladder transfer to $2\nu_2$ and $2\nu_5$ is expected to occur within a few collisions, making energy available in the $\sim$2000 cm^{-1} region. The signal in this region may be due to fluorescence from these overtones or from the fundamentals ν_1 and ν_4. Fluorescence from the fundamental ν_1 is expected to be stronger than that from the overtones on the basis of the greater oscillator strength. The ν_4 band is much weaker[12]. In fact, no individual ν_4 fluorescence has ever been detected in the series CH_3X or CD_3X. The rapidity of the activation is consistent with a direct up-the-ladder process. However, ν_1 lies within 48 cm^{-1} of, and is in Fermi resonance with, $2\nu_5$, so it will be populated on the same time scale, by Eq. (3b). The population of ν_4, whether it proceeds directly from the overtones, Eq.(4), or via ν_1, Eq. (5), may be expected to be slower. It seems likely that the component of fluorescence from this level is weak compared to the total fluorescence in the 5μ region, in which case a slower rise would not be observable.

It is also worth mentioning that the 5μ signal shows a single fast rise followed by a double exponential decay. The second portion

of the decay is the V-T/R relaxation, but the first may well reflect V-V transfer into ν_4. While the small amplitude of this component precludes measurements on it, it is well separated from the measured 5μ rate constants, and probably has a value on the order of 100 $msec^{-1}torr^{-1}$.

The ν_6 level is favored over ν_3 for collisional activation from ν_2 or ν_5 for two reasons, the smaller energy deficit and the larger breathing sphere parameter. If Eq. (7) does indeed proceed much more rapidly than Eq. (6), ν_3 will probably be populated by Eq. (8), which involves a considerably smaller energy gap. We cannot rule out population of ν_3 via transfer from ν_2 and ν_5 into $2\nu_3$, but such processes involving overtones are generally expected to be an order of magnitude or so less efficient than processes involving fundamentals. The smaller energy defect would enhance the contribution of the overtone route, but the small breathing sphere parameter of ν_3 still leads us to favor the ν_2-ν_6 route. These expectations were borne out in the series of CH_3X and CD_3X works. No observation of a direct crossover from an overtone to another fundamental has ever been measured save for up the ladder V-V transfer. The latter processes are energetically favorable due to the very small energy defects (anharmonicities) involved.

It is interesting to compare the activation for the long-wavelength signals in CD_3Br, CH_3Br[8], and CH_3Cl[5,6] in light of the energy gaps and the breathing sphere parameters for the modes involved. In the last two species there is one level (ν_3) below the laser-excited level (ν_6). In CD_3Br, we assume that the process which occurs is ν_2-ν_6 transfer. The products of the appropriate breathing sphere parameters are tabulated in Table 2 along with the energy gaps and the experimental

TABLE 2

Activation of Low-Lying Levels

Species	Transfer Process Breathing Sphere Parameters (amu^{-1})		BSP Product ($x10^3$)	Energy Gap (cm^{-1})	Number of Collisions
CH_3Br	ν_6	ν_3			
	0.27	0.027	7.29	340	170
CH_3Cl	ν_6	ν_3			
	0.26	0.027	7.02	280	110
CD_3Br	ν_2	ν_6			
	0.091	0.13	11.83	280	77

results on the number of collisions required for the process. Notice that, in two cases in which the breathing sphere parameters are essentially identical, the smaller energy gap in CH_3Cl is reflected in the smaller number of collisions, while in the cases which exhibit equal energy gaps, activation proceeds in fewer collisions in CD_3Br, where the product of the breathing sphere parameters is larger.

The results on the deactivation of the 5μ states and the long wavelength states are consistent with a single deactivation process for all levels. All the measured V-V rates are at least several times faster than the deactivation, so the deactivation can most probably be pictured as proceeding via the lowest levels, ν_3 and ν_6, with energy feeding into these levels from the excited manifolds by the V-V processes. In such a case, approximate solution of the kinetic equations yields the result that the total deactivation rate is a weighted sum of the deactivation rates from ν_3 and ν_6, with the weighting factors being the Boltzmann probabilities of finding a molecule in either state.[2]

While ν_3 is lowest in energy, ν_6 is given nearly equal statistical weight by its double degeneracy, and may in fact be more important in the deactivation because of the larger breathing sphere parameter. Calculations based on SSH theory indicate that for CD_3Br itself, deactivation from ν_3 is approximately five times more significant than from ν_6, while for the rare gases, the ν_6 contribution is in fact fifty percent larger for helium, and decreases successively relative to the ν_3 contribution for the heavier collision partners.

The calculated results for the two levels are shown in Table 3, along with the appropriately weighted sum. That these results fail to

TABLE 3

Calculated Deactivation Probability

Collision Partner	ν_3 Probability per gas kinetic collision	ν_6 Probability per gas kinetic collision	Weighted Sum
CD_3Br	2.10×10^{-5}	4.22×10^{-6}	1.25×10^{-5}
He	1.49×10^{-2}	2.14×10^{-2}	1.82×10^{-2}
Ne	8.62×10^{-4}	4.92×10^{-4}	6.75×10^{-4}
Ar	1.70×10^{-4}	6.10×10^{-5}	1.15×10^{-4}
Kr	2.10×10^{-5}	4.64×10^{-6}	1.27×10^{-5}
Xe	7.13×10^{-6}	1.22×10^{-6}	4.13×10^{-6}

agree with the experimental values, particularly as to the variation through the rare gas series, should not be regarded as surprising. The theory is far from quantitatively reliable, and takes no account of V-R relaxation. This latter type of deactivation[16] is expected to yield rare gas rate constants which vary only slightly through the series - more in line with the observed behavior, and its contribution for self-relaxation would considerably enhance this value. The SSH calulations were performed primarily to gain some insight into the expected relative contributions of ν_3 and ν_6 to deactivation.

2.5 Conclusions

Collisional transfer of vibrational energy in CD_3Br has been studied in a continuing investigation of the CH_3X and CD_3X series. The pattern of energy transfer in CD_3Br is similar to that established in the CH_3X series, with relatively rapid distribution of excess energy among the vibrational levels preceding a considerably slower overall deactivation. Activation of the 5μ levels is very rapid, presumably reflecting up-the-ladder transfer; consideration of energy gaps and breathing sphere parameters, as well as comparison with similar processes in CH_3Br and CH_3Cl seems to establish the mechanism as a direct ν_2-ν_6 transfer. Deactivation probably involves significant contributions from both ν_6 and ν_3.

A few comparisons can be made with energy transfer rates in the CH_3X series considering the parameters of energy transfer theory. An example has been given in considering the activation of the low-lying

levels in CH_3Cl, CH_3Br, and CD_3Br. When work on the CD_3X series has been completed a detailed comparison of the behavior of the two series will provide additional tests of the validity of such considerations.

References

1. E. Weitz, G. W. Flynn, and A. M. Ronn, J. Chem. Phys. 56, 6060 (1972).
2. E. Weitz and G. W. Flynn, J. Chem. Phys. 58, 2679 (1973).
3. E. Weitz and G. W. Flynn, J. Chem. Phys. 58, 2781 (1973).
4. F. R. Grabiner, G. W. Flynn, and A. M. Ronn, J. Chem. Phys. 59, 2330 (1973).
5. J. T. Knudtson and G. W. Flynn, J. Chem. Phys. 58, 2684 (1973).
6. F. R. Grabiner and G. W. Flynn, J. Chem. Phys. 60, 398 (1974).
7. S. M. Lee and A. M. Ronn, Chem. Phys. Letters 22, 279 (1973).
8. B. L. Earl and A. M. Ronn, Chem. Phys. 12, 113 (1976).
9. Y. Langsam, S. M. Lee and A. M. Ronn (submitted to Chem. Phys.).
10. R. D. Bates, Jr., G. W. Flynn, J. T. Knudtson, and A. M. Ronn, J. Chem. Phys. 53, 3621 (1970).
11. E. W. Jones, R. J. L. Popplewell, and H. W. Thompson, Spectrochmiica Acta 22, 639 (1966).
12. A. D. Dickson, I. M. Mills, and B. L. Crawford, Jr., J. Chem. Phys. 27, 445 (1957).
13. J. L. Stretton, Trans. Faraday Soc. 61, 1053 (1965).
14. J. Aldous and I. M. Mills, Spectrochimica Acta 18, 1073 (1962).
15. W. T. King, I. M. Mills, and B. L. Crawford, Jr., J. Chem. Phys. 27, 455 (1957).
16. C. B. Moore, J. Chem. Phys. 45, 2979 (1965).

FIGURE CAPTIONS

Figure 1. Experimental setup

Figure 2. CD_3Br Vibrational Energy Levels

Figure 3. Deactivation of CD_3Br 5μ modes. The non-zero intercept is a reflection of expermental uncertainty, and does not correlate with the radiative lifetime, which is $\gtrsim$1 sec.

Figure 4. Deactivation and Activation of CD_3Br Low-Lying Levels. Large intercept in upper panel is due to presence of 90 Torr of Xe. Non-zero intercept in lower panel is not significant.

Figure 1

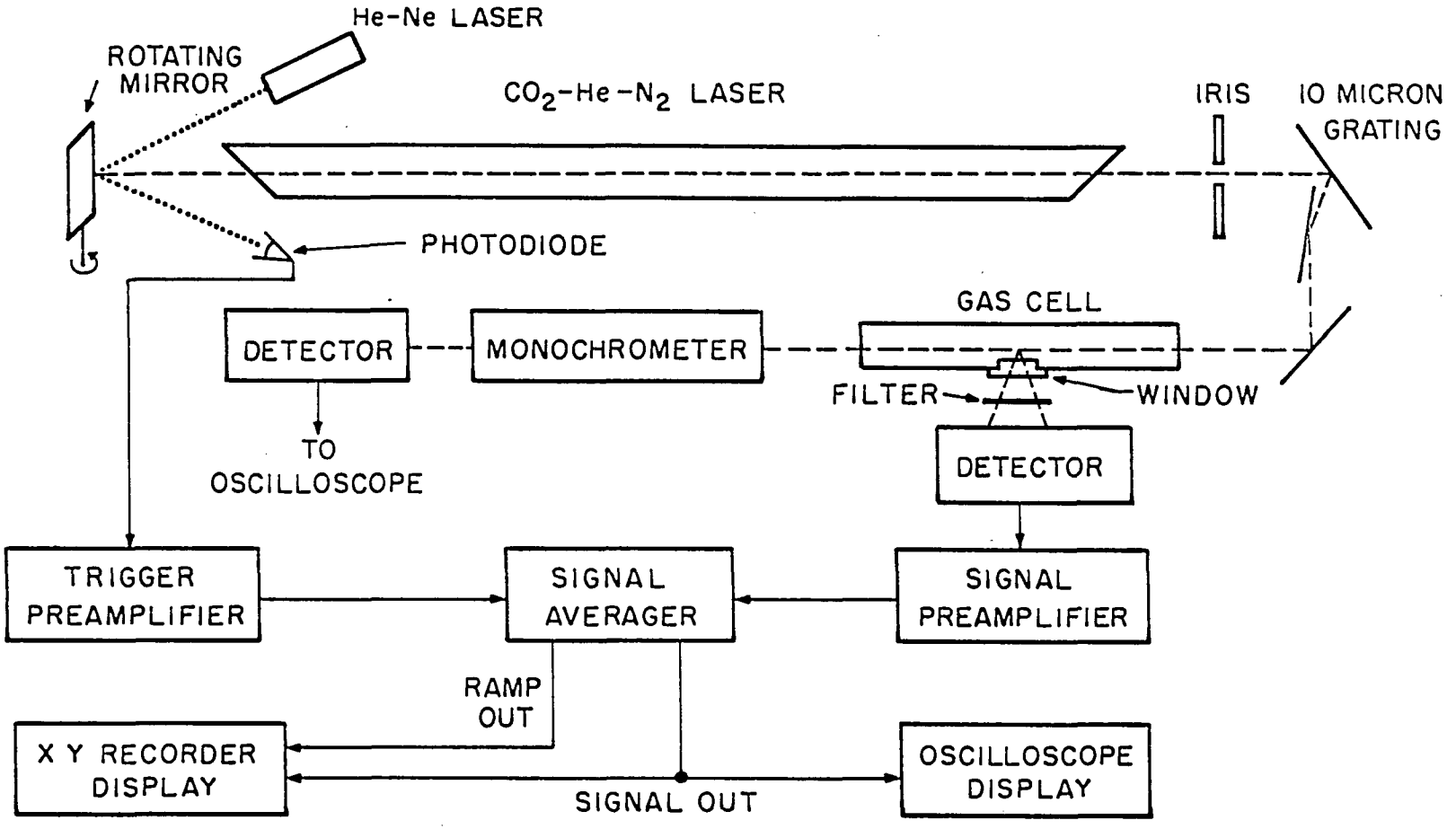
He-Ne LASER
ROTATING MIRROR
CO_2-He-N_2 LASER
IRIS
10 MICRON GRATING
PHOTODIODE
GAS CELL
DETECTOR
MONOCHROMETER
FILTER
WINDOW
TO OSCILLOSCOPE
DETECTOR
TRIGGER PREAMPLIFIER
SIGNAL AVERAGER
SIGNAL PREAMPLIFIER
RAMP OUT
X Y RECORDER DISPLAY
OSCILLOSCOPE DISPLAY
SIGNAL OUT

Figure 2

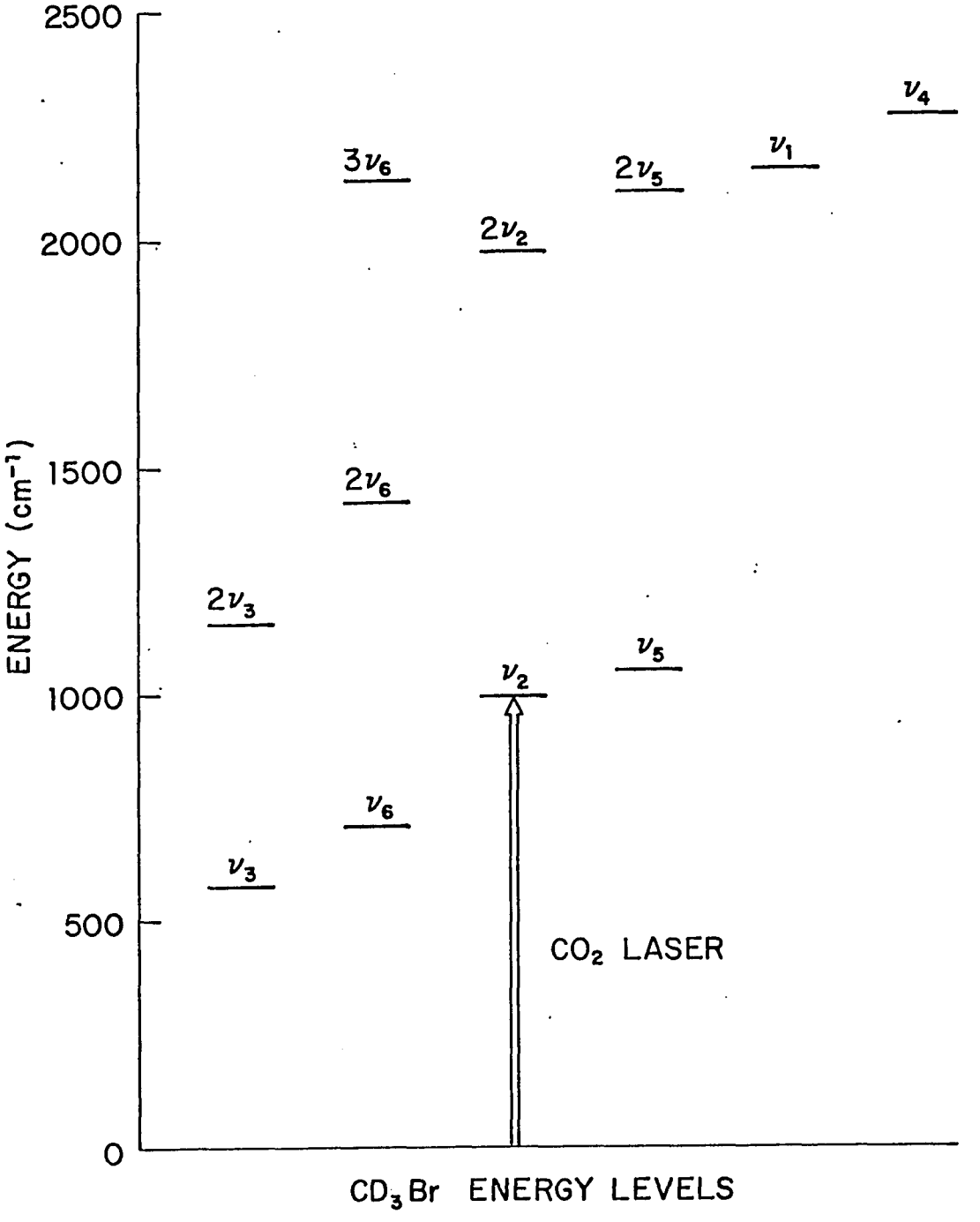
2500
2000
1500
1000
500
0
ENERGY (cm⁻¹)
ν_4
ν_1
$3\nu_6$
$2\nu_5$
$2\nu_2$
$2\nu_6$
$2\nu_3$
ν_5
ν_2
ν_6
ν_3
CO_2 LASER
CD_3Br ENERGY LEVELS

Figure 3

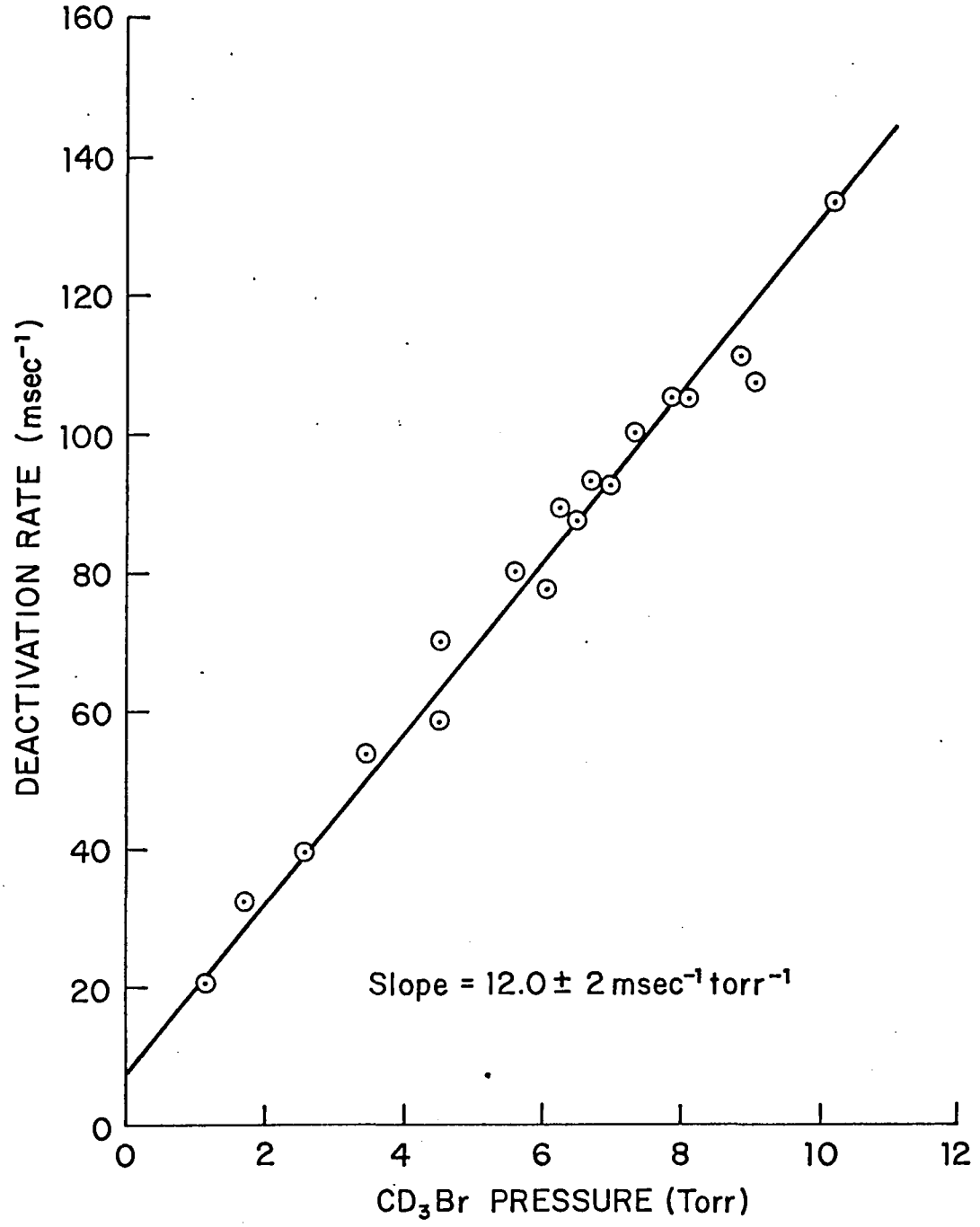
160
140
120
100
80
60
40
20
0
DEACTIVATION RATE (msec⁻¹)
Slope = 12.0 ± 2 msec⁻¹ torr⁻¹
0
2
4
6
8
10
12
CD₃Br PRESSURE (Torr)

Figure 4

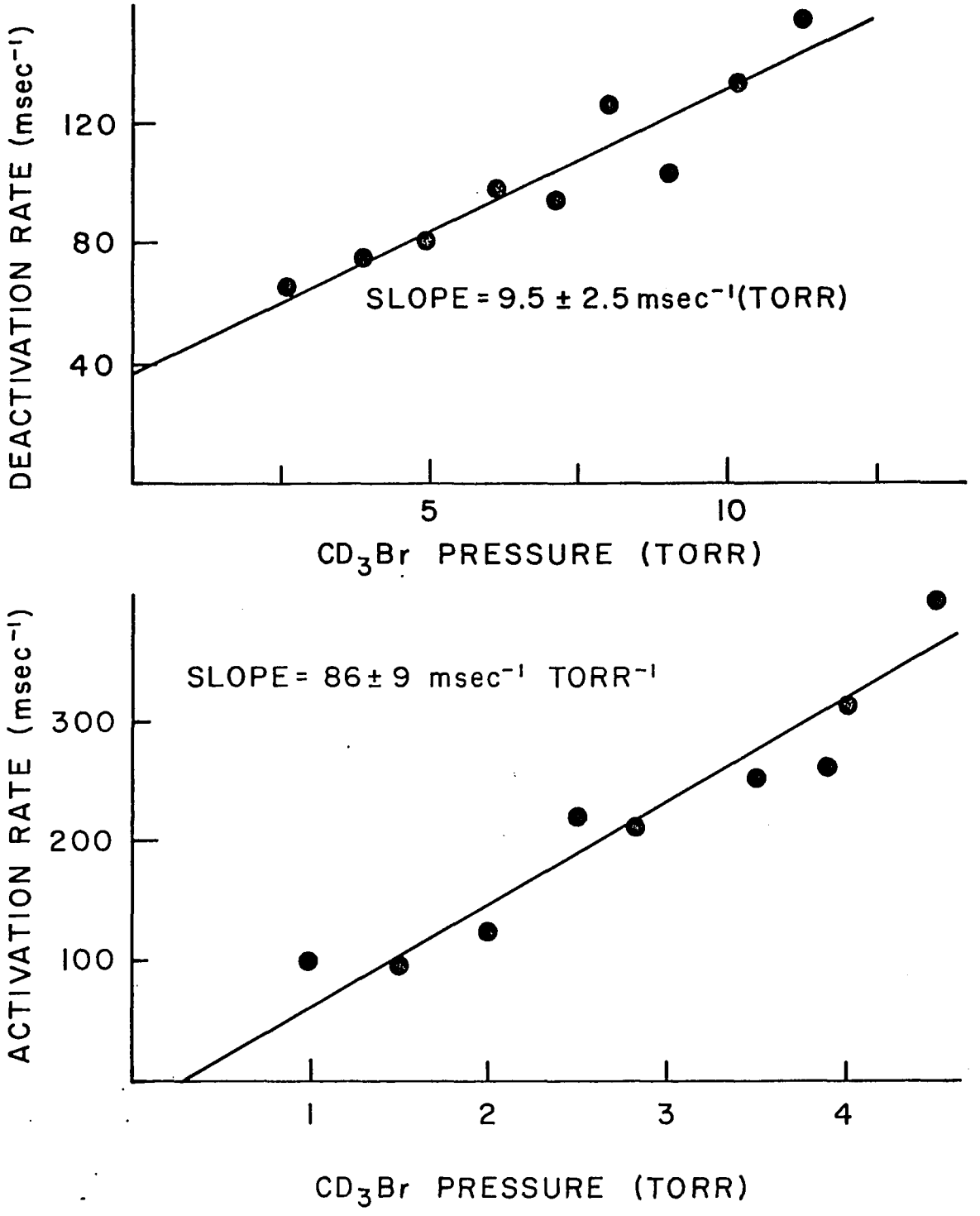
DEACTIVATION RATE (msec⁻¹)
120
80
40
SLOPE = 9.5 ± 2.5 msec⁻¹(TORR)
5
10
CD3Br PRESSURE (TORR)
ACTIVATION RATE (msec⁻¹)
300
200
100
SLOPE = 86 ± 9 msec⁻¹ TORR⁻¹
1
2
3
4
CD3Br PRESSURE (TORR)

Chapter 3

BUILDING A CO_2 TEA LASER

3.1 Constructional details

The CO_2 TEA laser system is shown in Fig. 1. The main laser body, made of 9.5 cm i.d. by 10.7 cm o.d. plexiglass tubing 76 cm long, is seated on two V-shaped wood stocks. These wood stocks were fixed on the adjustable seats which are movable on an optical bench. Both ends of the tubing were flanged and O-ringed with 4 cm long, 2.5 cm i.d. by 3.8 cm o.d. plexiglass tubings in which the movable NaCl windows were locked in with a Brewster's angle.

The Rogowski profile aluminum electrodes (4 cm x 60 cm x 2 cm, Tachisto Inc.) were mounted inside the tubing with a 1.9 cm spacing. This was done by means of adjustable vacuum-tight mounts which threaded through the copper plates outside the tubing. On the top copper plate, there were mounted 12 sprague door knob capacitors (30 KV, 500 pF each, 30DKT500, H.L.Dalis Inc.) which were connected with 12 strips of copper. On the other ends the copper strips were screwed onto the spark plugs (L77V, Champion). The bottom copper plate which is grounded was also built the same way as the top one but those copper strips were attached to the ground end of the spark plugs on the plexiglass tubing.

The pulse transformer (100:1, U.S. Scientific Instruments), charging and discharging resistor (50 KΩ), oil discharge capacitor (50 KV, 0.05 μF, Condenser Products Corp.) and demountable pressurized

spark gap (0-30 PSIG, 12-50 KV, SG501, Tachisto Inc,) were all mounted in a grounded lead box for minimizing inductance. The box and the laser tubing except the protructing NaCl windows were put in a grounded copper network cover for protection and reduction rf noise.

The timing and trigger generator (model 050C, Tachisto Inc.) was used in conjunction with the pulse transformer. This generator produced synchronization and triggering signals can be tuned with the repitition rate from 0.1 to 100 pulses/sec. A manual signal pulse push button was also provided. The dc power supply was 50 KV, 70 mA obtained from Universal Voltronics.

The 200 cm optical cavity was formed by a polished 50mm flat beryllium-Copper mirror and a IR grating (75 grooves/mm, 38 mm x 10 mm original on polished copper substrate, ML301, PTR Optics Corp.) The IR grating and an additional mirror were seated on an optical plate so that the grating can be rotated and adjusted vertically. Therefore, most of rotational lines of the 001-02^{0}0 (9.6 μm) and 001-100 (10.6 μm) bands of CO_2 vibrational transition are available by rotating the grating. The plane mirror, providing an additional reflection to prevent the direction of the output beam from changing as the laser is tuned through various wavelengths, was set at an angle approximately 50^{o} to the grating. The BeCu mirror reflector can also be turned vertically and horizontally, so that optical line-up is easy to obtain.

3.2 Operational details

The flow rates of the gases, CO_2, He and N_2, were controlled

by individual needle valves at the fixed pressure and were mixed in a mixing manifold before flowing into the discharge chamber. The ratio of the mixture of gases was not measured but optimized by adjusting the individual valve so that the uniform discharge was obtained at the applied voltage. It was found that the uniform discharge is obtained with the following number of turns on the valves of CO_2:He:N_2 approximately equal to 5 : 10.5 : 5.5 at the fixed inlet pressure of 10 PSIG. The preionizer, triethylamine, carried by the He gas was added in order to prevent arcing and to obtain a stable output energy. The gas mixture is introduced into the discharge tube from the center and is let out at both ends.

A pulse energy of 3J was obtained in a multimode condition at an applied voltage of 27 KV. The area of the output beam was 1.5 cm by 1.0 cm and the typical pulse length had the full width at half maximum of 300 ns with a tail of 700 ns. The tail of the pulse contains about one-third of the total energy. It has been reported that the tail is due to the slower buildup of the higher order transverse modes[1]. Therefore, the laser can be constrained to fundamental mode operation with the narrowness of the pulse half-width and the disappearance of the tail at sacri fice of the output power (more than 50 percent). At the operational parameters described above, the peak intensity is about 5MW/cm^2 in a multimode condition. This intensity is still not sufficient to induce most chemical reactions, therefore, a focal lens is always needed to increase the power intensity. When a 5 inch focal length ZnSe lens is used, there is a 100-fold increase in intensity so that air breakdown on both sides of the lens was observed. The front breakdown is due to the energy reflected from the uncoated focussing lens.

3.3 Discussion

Several similar devices of CO_2 TEA lasers have been reported[1-4]. The one described here is an inexpensive, simple and tunable, particularly useful for laboratory research and in studies of the laser induced chemical reactions. The performance of this laser is exceptionally good, up to now at least one hundred thousand pulses have been obtained and no degradation is apparent. The output energy is always very stable even after continuous excitation with ten thousand pulses—the largest number of irradiation pulses that had been used at one time. However, to maintain the laser in a high efficient performance condition care must be taken with optical components and some electronic devices as discussed below:

(a) NaCl windows: When the laser is not in use NaCl windows are always covered with plastic bags, in which a drying agent is provided, this keeps the windows dry and clean. Periodically, the windows are either cleaned by lens paper moistened by dry alcohol or acetone or changed with new ones.

(b) Resonators: They are also covered with plastic bags when they are not in use. Since the optical amplification is very sensitive to the surfaces of the resonators, the damaged or dirty surfaces of the resonators cause great reduction of the output power. Hence, before operating the laser the He or N_2 gas is used to blow the surfaces of the resonators to keep dust-free.

(c) Electrodes: The electrodes are needed to be repolished after a certain period, usually once a year, for cleaning the solid deposits on

the surfaces of the electrodes.

(d) Pressurized spark gap: The spark gap must be cleaned frequently since breakdown of the filled N_2 gas in the spark gap eventually contaminates the surfaces. To apply higher voltages the spark gap also needs to be refilled to the suitable pressures to achieve a constant discharge.

References

1. P.R. Pearson and H.M. Lamberton, IEEE J. Quant. Electron. QE-8, 145 (1972).
2. A. J. Beaulieu, Appl. Phys. Lett. 16, 504 (1970).
3. A. K. LaFlamme, Rev. Sci. Instrum. 41, 1578 (1970).
4. H. J. Seguin, K. Manes and J. Tulip, Rev. Sci. Instrum. 43, 1134 (1972).

Figure 1 Caption

The schematic diagram of CO_2 TEA laser.

Figure 1

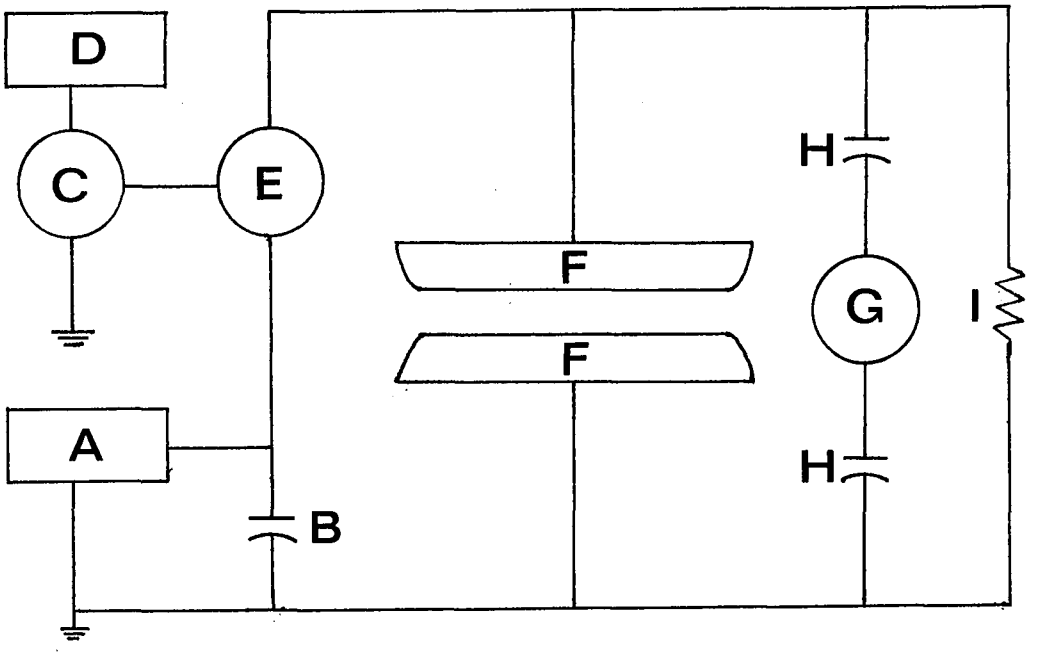

A. High voltage dc power supply (50 KV, 70 mA)

B. Discharge capacitor (50 KV, 0.05 μF)

C. Pulse transformer (100:1)

D. Timing and trigger generator (0.1 to 100 pps)

E. Pressurized spark gap (0-30 PSIG, 12-50 KV)

F. Rogowski profile electrodes (aluminum)

G. Spark plugs (Surface gap, L77V Champion)

H. Trigger capacitors (30 KV, 500 pF each)

I. Charging and discharging resistor (50 KΩ)

Chapter 4

LASER INDUCED MULTIPHOTON ABSORPTION AND GAS BREAKDOWN

4.1 Introduction

CO_2 infrared lasers can be used as sources to induce or catalyze chemical reactions. Traditional photochemical reactions are usually initiated by uv or visible light sources. These posess inherent high photon energy and as such drive the reactions via electronic excitation. The infrared laser light on the other hand has low photon energy (2.3 Kcal) sufficient only to vibrationally excite the reactant molecule. However, it has been shown that at sufficiently high fluences (energy/cm^2) chemical reactions can be driven efficiently. Depending on the excitation processes, a chemical reaction can be induced in two different ways. One is the energy transfer from a laser photon to a reactant molecule through multiphoton absorption mechanism usually termed an "on resonance" process. The necessary condition for this mechanism is a matched particular vibrational frequency of the reactant molecule with the laser frequency. The other process, so called "off resonance", occurs by gas breakdown caused by the very high intensity of the electromagnetic field. In this process, the plasma (spark) generated through avalanche ionization by means of breakdown is driven by inverse bremsstrahlung heating of the electrons. Chemical reactions that occur via this process are expected to show similar characteristics to high temperature reactions. In this chapter, the proposed theoretical models for multiphoton absorption and

gas breakdown processes will be reviewed.

4.2 Multiphoton absorption

A Q-switch CO_2 laser with power intensity of about 10^3 W/cm^2 is usually used to investigate collisional vibrational energy transfer by monitoring the fluorescence signals from excited molecules. Consequently, after sample molecules are excited by the laser light on resonance and with a 1 photon per molecule absorption limit, they return to the ambient conditions via collisional processes. The nature of such vibrational energy transferring collisions are well understood. However, few if any chemical reactions can be induced at such power levels. This implies that vibrationally excited molecules can not acquire sufficient energy, either through further absorption of laser photons or by collisional effects, to overcome typical energy barriers for chemical reactions at these fluences. Whereas a TEA CO_2 laser with power intensity higher than 10^6 W/cm^2 can initiate the chemical reaction in many known instances. Therefore, at such a high energy density the reactant molecule is expected to absorb more photons than the usual one and decompose either collisionlessly or on subsequent collisions. It has been demonstrated that many such systems exist, for example, SF_6 can be decomposed collisionlessly and still maintain isotopic selectivity leading to an achievement of highly efficient isotope separation[1]. These experimental findings are however not easily explained theoretically. Difficulties arise due to inherent anharmonicity of vibrational states and the monochromaticity of the existing laser light. The

intrinsic question, that is, how does a sample molecule acquire enough energy from the infrared photons to dissociate into separate fragments, while simultaneously keeping the absorption resonant enough for isotopically selective dissociation to occur? Two different models have been proposed to interprete the mechanism of many photon absorption for the dissociation of an isolated molecule.

The first explanation[2] is based on a combination of the effect of "triple vibrational-rotational resonance" with the effect of nonresonant absorption at the transitions in the "vibrational quasi-continuum" of a polyatomic molecule. The second model[3] is basically the same as the first one except treatments of the lowest vibrational transition regime. A number of terms must be defined and explained before a quantitative description of these models are attempted.

(i) The Stark effect: In the large electric field present in the TEA CO_2 laser radiation absorption line broadening, due to a splitting of molecular vibrational-rotational sublevels, occurs. This broadening is a result of the dynamical Stark shift which can partially offset the anharmonicity of vibrational levels. For a diatomic molecule (rigid rotor approximation), the magnitude of the splitting is given by the equation[4]

$$\Delta\bar{\nu} = (B_e/2)(\mu E/h\nu)^2, \text{ cm}^{-1}$$

where B_e is the rotational constant in cm^{-1}, μ is the transition dipole moment in Debye, E is the electric field strength, and ν is the laser frequency. This frequency shift is dependent on the second order of

the field strength. For molecule such as SF_6 the numerical value is less than 0.1 cm^{-1} for μ (ν_3) ~0.3 D, B_e ~0.03 cm^{-1} and electric fields of the order of 10^8 V/cm. However, this effect would be increased substantially for a molecule with larger dipole moments and rotational constants.

(ii) Power broadening: The multilevel power broadening arises because a transition between oscillator levels occurs in a time which is short compared to the time in which laser field gets out of phase with the oscillator. This effect is determined by the Rabi frequency[4] and the detuning $\nu-\nu_o$, where ν is laser frequency and ν_o is oscillator frequency. The Rabi frequency is defined as

$$\nu_R = \mu E_o/h$$

where E_o is the time independent field strength, μ is the transition dipole moment and h is the Planck's constant. The excitation of the oscillator is proportional to the square of the term, $\nu_R/(\nu-\nu_o)$, at the maximum. Therefore, if the Rabi frequency is large compared to the detuning $(\nu-\nu_o)$, there will be a significant excitation. Take the example of SF_6 for numerical calculation, the Rabi frequency at a field strength of 10^6 V/cm is approximately 5 cm^{-1} for the ν_3 mode (μ ~0.3 D). This is clearly a much larger effect than the Stark effect. If the anharmonicity of the pumped vibrational level is small compared to the Rabi frequency then very high vibrational levels can be populated in very short times.

In view of these two definitions let us return to the discussion

of the proposed models. Both models separate the vibrational energy levels in the ground electronic state into three regions which are characterized by coherent, incoherent and continuum states, respectively. The lowest levels represent the coherent regime, the quasi-continuum or incoherent excitation form the middle of the ladder and the true continuum represents the true dissociation limit. The model called "triple vibrational-rotational resonance" or "PQR transition" attempts to explain that the first three consecutive vibrational excitation levels of a molecule can be resonant with the laser frequency solely by compensation to the anharmonicity by changing the rotational states. The laser frequency is tuned to match with the Q-branch of the transition from ν=1 to ν=2. Therefore, the vibrational anharmonicity can be overcome by compensation for the anharmonic shift of the transition energy by a change in the rotational state. After the polyatomic molecule is excited to ν=3, the density of the levels becomes high enough so as to form a quasi-continuum region where energy levels overlap one another. Excited molecules in this regime therefore can directly absorb enough photons, if the power is high enough, without requiring a resonant field to reach the continuum dissociation limit in the ground electronic state. This model shows that molecular decomposition depends on the power density rather than power intensity since the PQR transition requires only a power intensity of about 10^5 W/cm^2 for a molecule, such as SF_6, with a rotational constant of $\sim$0.03 cm^{-1} and dipole moment $\sim$0.3 D. Therefore, the decomposition rate is controlled by acquiring a sufficient energy from the quasi-continuum states to reach dissociation limit.

For a molecule with less dense vibrational levels such as BCl_3,

however, the above model can not apply. Therefore, the model introduces a refinement by allowing the excited molecules after having undergone the PQR transition to "leak" into the quasi-continuum states and then reach dissociation limit by subsequent absorption.

Depending on the peak power, the second model assumes that the coherent region can be excited to higher levels in the resonant field. Since anharmonicity is mostly overcome by Rabi frequency, the power intensity is more important than power density in this region. In the incoherent region, without relation to any particular mode it is assumed that all the vibrational degrees of freedom are at the same temperature. The RRKM theory[5] is then applied and the familiar Arrhenius equation provides the quantitative rate calculation for this unimolecular dissociation. Region III is the true continuum of the levels above the dissociation limit. Dissociation may occur during and after the laser pulse, before de-excitation by collisions can take place.

The introduction of RRKM theory into laser induced reactions is significant since it is always argued that laser energy may accumulate in a particular vibrational degree of freedom and lead to a very specific molecular decomposition. The inherent assumption of RRKM theory is that unimolecular dissociation occurs before a full vibrational period elapses. Otherwise, statistical distribution into all vibrational modes would ensue. A typical vibrational period is about 10^{-13} sec, i.e., if laser energy is deposited in the molecule in a period shorter than this vibrational period the energy could accumulate in a particular vibrational degree of freedom (ignoring the rotational relaxation). However, the laser energy contained in such a short period is very small compared

with the full laser pulse. The probability that this small part of the pulse can induce a molecular decomposition is quite low. Additionally, it should be independent of collisional events at moderately high pressures. From the results shown in laser isotope separation experiments with SF_6 and others it is clear that good separation occurs in the low pressure regime and that collisional scrambling is obviously a critical factor.

Collisional effects are important for multiphoton absorption processes, since the collision number may be large within the time span of a laser pulse (typically 0.1 to 1 μs). Energy transfer by collisional activation or deactivation within a laser pulse always plays an important role. The following experimental results show the significance of this collisional effects. Benzene is transparent to irradiation with P(20) 10.6μ laser line at pressures under 40 torr. In a system comprising 6 torr of benzene and 1 torr of SF_6, however, carbon was found deposited over the whole cell when the same irradiation was attempted. A tremendous energy transfer cross section thus drives benzene at least as high as the quasi-continuum states from which decomposition is non-resonant.

To summarize, comparison between these two existing models based on the calculated energy level density in a particular vibrational mode increases exponentially with increasing energy states. In SF_6, for example, the density of states is about 0.1 per cm^{-1} at 0.1 eV, about 10 per cm^{-1} at 0.2 eV and more than 100 per cm^{-1} at 0.4 eV.[2] However, level density is expected to greatly increase after coupling with inactive vibrational modes which may become active subsequent to the

repopulation by the initial exciting photon. Furthermore, Stark effect, power broadening and collisional broadening would play important roles in compensating for vibrational anharmonicity. Experimentally, we will show in Chapter 5 that efficient rotational relaxation can enhance the dissociation rate of SF_6. Therefore, a power intensity dependence in a coherent region, as proposed in model II for multiphoton absorption processes, should be favored over that dependence calculated by model I (PQR model) for multiphoton collisionless dissociation.

4.3 Gas breakdown

Gas breakdown is defined as the sudden onset of a electrical conductivity in a normally non-conducting gas. This occurs due to the existence of free electrons in the medium. Laser induced gas breakdown is always accompanied by intense emissions of light, lasting longer than a laser pulse duration with a characteristic afterglow. This plasma is essentially opaque to any subsequent laser radiation. The mechanism responsible for initiating the breakdown has been investigated and a number of models are proposed. The avalanche breakdown mechanism[6] presumes the existence of initial electrons which are accelerated via the high electromagnetic field by inverse bremsstrahlung[7] until they acquire sufficient energy to ionize the gas molecules(or atoms) collisionally. The process repeatedly continues with the new electrons generated by ionization and gives rise to an avalanche resulting in showing an exponential rate of growth of the ionization. Another model assumes that no electron exists previous to the introduction of the laser field and

that the latter causes ionization by multiphoton mechanism[8]. There also exist theories based on mixed mechanisms[9]. The multiphoton ionization process requires that the number of photons of energy sufficient to ionize an atom (or molecule) are absorbed directly by the atom (or molecule). Since this process depends on the joint probability of absorbing M photons, the ionization rate is proportional to the laser intensity raised to the M-th power. This was shown to be important for the breakdowns observed with extremely short-duration laser pulses focussed in gases at low pressure since breakdown fields of 10^8 V/cm favor this theory. At higher pressures the breakdown threshold of about 10^5 V/cm for CO_2 laser radiation favors the avalanche mechanism because the longer wavelength results in lower thresholds in this model[7]. However, it should be emphasized that, in order to induce the avalanche ionization process, it is necessary that the process be initiated by some other mechanism to provide the initial electrons, e.g., exoelectrons, etc.

To explain the existence of the initial electrons during the early stages of ionization in the avalanche model, a simple experiment was attempted. (a) The initial free electrons are provided through photoionization by multiphoton mechanism[10]. Later experiments[11] showed that, for multiphoton ionization to be the trigger process, it must creat a free electron in the focal volume in approximately one nanosecond. The photon flux required to produce initiation is still too large as compared with the observed experimental breakdown fluxes. No conclusions were thus favored. (b) The initial electrons are produced by direct electron-tunnelling[12]. At high laser intensity, direct electron-tunnelling may produce the initial electrons for an avalanche.

Since the tunnelling probability is a very sensitive function of electric field, the plasma will tend to nucleate at a well defined intensity in the center of the focal region. However, the laser intensity required in this process may be as high as 10^{12} W/cm^2. Therefore, it would not be suitable to explain the plasmas induced by low laser intensity.

There also exists a probability that the initial electrons are available due to external sources, i.e., exoelectrons, cosmic, light, etc. Therefore, the avalanche ionization process would only depend on the field necessary to build up a certain critical number of ion pairs at the focus within the pulse duration. Since the mean energy gained per mean free path by an electron is function of E^2 (E represents the field strength), the number of ion pairs produced by an electron in time t should depend on E^2t.[13] This may explain the general correlation between the laser pulse shape and the time required for a visible discharge to occur. That is, the weaker the power intensity, the longer the time for observable breakdown.

Since breakdown can occur without matching the laser frequency with the vibrational frequency of the reactant molecule, the gas is effectively transparent to the laser light. However, when plasma is formed the motion of the electrons and ions in specific electrostatic oscillations is characterized by the plasma frequency (Langmuir frequency) ν_p. The equation of motion which defines the frequency ν_p of the electrostatic oscillation of the electrons leads to the relation[7]

$$\nu_p^2 = 4\pi e^2 n_e / m_e \qquad (1)$$

$$\nu_p \ (\text{sec}^{-1}) \ = \ 5.65 \times 10^4 \ [n_e \ (\text{cm}^{-3})]^{1/2}$$

where e, m_e and n_e are charge, mass and density of electron, respectively. The essence of a plasma oscillation is as follows, from the wave equation for monochromatic fields and induced plasma current densities, the dispersion results in the complex refractive index $\tilde{n}$, the relation[7] obtains

$$\tilde{n}^2 \ = \ 1 - \frac{\nu_p^2}{\nu^2(1 + i \ \nu_e/\nu)} \qquad (2)$$

where

ν = frequency of the electromagnetic wave,

ν_e = collision frequency between the fluids,

i = imaginary unit.

For a collisionless plasma(ν_e=0), the refractive index vanishes at the plasma frequency ν_p equals the laser frequency ν. The plasma is transparent only if $\nu > \nu_p$; otherwise the incident electromagnetic wave is totally reflected by the plasma. The frequency $\nu = \nu_p$ is called the critical frequency and is related by equation (1) to a special electron density of the plasma, called the critical density. Thus, at the critical frequency total energy absorption occurs. For the CO_2 laser frequency, the critical density is 10^{19} electrons/cm^3 according to equation (1). If the density of the plasma is higher than the critical density the plasma should then be totally reflecting just like a metal surface

(the solid state density of deuterium is 5.8×10^{22} cm^{-3}). For the absorption mechanism, theorists proposed two different types of models, nonlinear parametric interaction[14] and linear resonant interaction[15]. It is generally agreed that the energy absorption take place in the narrow critic layer where the plasma frequency ν_p equals the laser frequency ν. Therefore, there will exist a critical pressure for any gas that will correspond with the resonance regime where the critical electron density is 10^{19} cm^{-3} at CO_2 laser frequencies. This critical pressure depends on the charge state of the positive ions which are formed. Experimental results showed that this critical pressure is 300 torr for He about three times that of the threshold pressure to induce the breakdown[16].

Some general phenomena of laser induced plasma are described here.

(i) Plasma features: The structure of the plasma is a strong function of the available laser power and the optical arrangement used to focus the radiation. In general, at the center of the plasma is an extreme intense core. Surrounding this core is a region of lesser intensity which is generally divided into lobes. In this relatively low-intensity region, the critical layer appears as a moving front, where the resonant laser-plasma interaction actually occurs[16]. Outside this second region, there is a structureless cloud probably made up of excited atoms rather than ions and electrons[17]. This is because the fast, high energy electrons have very high diffusive loss rate to the wall and the surrounding gases prevent the generated ions from free motion.

The angular distribution of incident laser light scattered by

the plasma showed that the scattering is strongly peaked in the forward direction, with a lesser peak in the backward direction. The forward scattering may be due to Thomson scattering from free electrons or reflection from the dense plasma or both[17].

(ii) Threshold laser power density: Gas breakdown threshold is defined as the minimum laser radiation intensity required to produce the breakdown plasma such that an intense, visible spark is observed at the focus of a lens. The power density required for breakdown is given as[18]

$$(P/A) = \frac{2\, m_e\, \epsilon\, c\, I_p\, \nu^2 \ln(n_e/n_o)}{e^2\, \nu_e\, \tau} \qquad (3)$$

where

P = radiation power,

A = area,

m_e = electron mass,

ϵ = free space permittivity,

c = velocity of light,

I_p = ionization potential of the gas,

ν = radiation frequency of the field,

n_e = final electron density,

n_o = initial electron density derived externally or independently of the avalanche process,

e = electronic charge,

ν_e = electron-atom (molecule) collision frequency,

τ = duration of the laser pulse.

This expression is a simplified solution, yet, still shows qualitatively the dependence of the threshold on the various experimental parameters for the preferred avalanche process.

The threshold power is variable with different gases at different pressures. For a gas at constant pressure the threshold power is affected by external preionization. Preionization by dc electrical discharge reduces the threshold laser power[18] and shortens the duration of laser pulse being cutoff by the breakdown plasma[19]. This is because the initial electrons needed for an avalanche ionization were provided by the injection of free electrons into the focal volume.

Equation (3) predicts that the threshold power density is proportional to ν^2/τ, the experimental results showed that the agreement is within the error associated with such threshold measurements[18]. However, experiments designed to test the dependence of pulse duration on the power density led to the results that factors such as diffusion of the electrons out of the beam and/or inhibition of breakdown due to resonant absorption by the gases[20] must also be considered. The latter can be understood, as mentioned earlier, by considering the number of ion pairs produced by an electron in time t. As shown in the earlier discussion, ion pair formation should depend on E^2t, for a large production of ion pairs during breakdown obtained with CO_2 laser of moderate power, t must be long so as to maximize the product E^2t. However, τ, the laser pulse width, must be much larger than t so as to ensure high ion pair formation. Since E and τ are inversely proportional some preferential values must be found experimentally to satisfy both conditions. Usually, gas breakdown is induced by means of focussing the

laser beam directly into the gas cell therefore increasing the power density. In a high power intensity of the focal spot the electron can gain the energy and diffuse out of this very small spot very quickly and thus the relative rate of gain to loss affects the avalanche ionization. For a fixed divergence and initial beam size the focal spot diameter is directly proportional to the focal length of the lens. If the beam diameter is larger, there exists a higher probability for keeping the electrons in the beam and thus increasing the rate ratio of gain to loss. Therefore, the threshold would decrease as the focal spot size was increased.

The multiphoton ionization theory would predict a pressure dependence of $P^{-1/M}$, i.e., the threshold power density is not sensible to the pressure. Whereas the avalanche mechanism, as can be seen from equation (3), predicts the threshold has a P^{-1} dependence since ν_e which is the electron-molecule (atom) collision frequency is directly proportional to pressure P. Experiments with a CO_2 laser qualitatively showed that the threshold exhibits a P^{-1} dependence[18] as equation (3) predicts. This result provides additional evidence that breakdown induced by a CO_2 laser favors the avalanche mechanism.

(iii) The behavior of threshold pressure at a constant power intensity: There exist different threshold pressures for different molecular species. Below a threshold pressure the gas does not show optical breakdown because of the collisional heating rate can not overcome the diffusive loss rate of electrons. Threshold pressure conditions are intimately linked to the gas properties such as polarizability, dipole moment and ionization potential. Increasing the polarizability and dipole moment

or decreasing in the ionization potential will cause the threshold pressure to decrease. These results although qualitatively correct over a large range of species still do not allow a precise quantitative dependence determination. That is so since threshold pressures can be reduced by existence of impurities, preionization and application of external magnetic field. In the presence of impurities such as dust particles, the plasma nucleates strongly at such localities and expands in the form of an optical detonation wave[21], therefore, the threshold pressure is largely reduced. With a dc electrical discharge, the threshold pressure also decreases dramatically. Experimental results show the threshold pressure being reduced from 22 torr to 9 torr in OCS when a preionizing spark was supplied in addition to the TEA laser pulse. In SF_6 the threshold pressure decreased from 20 torr to 10 torr. Applications of a magnetic field will also reduce the diffusion rate normal to the field, thus increasing the time that electrons dwell in the focal region and lowering the breakdown threshold[22].

References

1. E. Fuβ and T. P. Cotter, Appl. Phys. 12, 265 (1977) and references there in.

2. R. V. Ambartzumian and V. S. Letokhov, Accounts Chem. Res. 10, 61 (1977).

3. J. G. Black, E. Yablonovitch, N. Bloembergen and S. Mukamel, Phys. Rev. Lett. 38, 1131 (1977).

4. J. P. Aldridge, J. H. Birely, C. D. Cantrell and D. C. Cartwright, Laser Photochemistry, Tunable Lasers, and Others Topics (Physics of Quantum Electronics, Vol. 4), S. F. Jacobs, M. Sargent III, M. O. Scully and C. T. Walker, Eds., Addison-Wesley, Reading, Mass.

5. P. J. Robinson and K. A. Holbrook, Unimolecular Reactions, Wiley-Interscience, New York, 1972.

6. J. P. Wright, Proc. Phys. Soc. 84, 41 (1964).

7. H. Hora, Laser Plasma and Nuclear Energy, Y. Ksander, Ed., Plenum, New York 1975.

8. T. B. Bystrova, G. S. Voronov, G. A. Delone and N. B. Delone, JETP Letters 5, 178 (1967).

9. R. Papoular, Laser Interaction and Related Plasma Phenomena, Vol. 2 H. Schwarz and H. Hora, Eds., Plenum, New York, 1972.

10. H. B. Bebb and A Gold, Phys. Rev. 143, 1 (1966).

11. R. G. Tomlinson, Phys. Rev. Lett. 14, 489 (1965).

12. L. V. Keldysh, Sov. Phys. JETP 20, 1307 (1965).

13. M. M. Shahin, Reactions Under Plasma Conditions, Vol. I, M. Venugopalan, Ed., Wiley-Interscience, New York, 1971.

14. M. N. Rosenbluth, R. B. White and C. S. Liu, Phys. Rev. Lett. 31, 1190 (1972).

15. R. P. Godwin, Phys. Rev. Lett. 28, 85 (1972).

16. E. Yablonovitch, Phys. Rev. Lett. 35, 1346 (1975).

17. M. Young, M. Hercher and C. Y. Wu, J. Appl. Phys. 37, 4938 (1966).

18. D. C. Smith, J. Appl. Phys. 41, 4501 (1970) and references there in.

19. H. S. Kwok and E. Yablonovitch, Appl. Phys. Lett. 27, 583 (1975).

20. D. C. Smith, Appl. Phys. Lett. 19, 405 (1971).

21. Yu. P. Raizer, JETP Lett. 7, 55 (1968).

22. D. R. Cohn, C. E. Chase, W. Halverson and B. Lax, Appl. Phys. Lett. 20, 225 (1972).

Chapter 5

LASER ISOTOPE SEPARATION IN SF_6

5.1 Introduction

Sulfur hexafluoride has been the focus of a large number of investigations and experimental studies of Laser Induced Isotope Separation (LIS) of SF_6 via multiphoton absorption have concentrated on this species due to its inherent similarity to the uranium analog.

This particular investigation was undertaken with the hope that some additional light might be shed on two specific issues, still grey, involving the mechanism of laser induced dissociation in polyatomic species via multiphoton absorption. The first issue dealt with here is the effect of laser pulse duration and number with respect to the dissociation of both ^{34}S and ^{32}S species. The second and the more complex issue of collisions and their role in the dissociation was addressed in a series of experiments involving different collision partners and pressure regimes.

5.2 Experimental

A Rogowski type TEA CO_2-N_2-He laser, built in our laboratory, tuned to P(20) of 10.6 μm was the excitation source for all measurements.

A preionizer was used to obtain a stable output. The output of this line was set at 2J with a pulse duration of 1 μs. The pulse shape

was of 300 ns full width at half height and a tail of 700 ns. The repetition rate of 50 pulses per minute was used. The laser output was focussed with a 5 inch focal length ZnSe lens giving an irradiation volume of approximately 0.40 cm^3 inside the sample cell. The sample cells were of glass, each having a volume of 18 cm^3, 10 cm long and 1.44 cm i.d., fitted with NaCl windows. Gases were Matheson research grade and used without further purification.

Product analysis was carried out by grating infrared absorption spectroscopy as slow scan rate with a Perkin-Elmer Model 267. The peak at 947.9 cm^{-1} is due to absorption by the ν_3 fundamental of $^{32}SF_6$, the shoulder at 930.5 cm^{-1} due to the $^{34}SF_6$ ν_3 absorption (see figure 1). At pressures of SF_6 higher than 0.4 torr the gases were expanded to a known volume before IR spectra were taken so as to avoid saturation of the peak at 947.9 cm^{-1}. When the pressures of SF_6 below .4 torr were used, the calculated percentages of species remaining as shown in Table 1 were made by direct comparison of the logarithms of the percent transmission subsequent ot laser irradiation with the logarithms of non-irradiated samples for a preset number of pulses. Calculated concentrations of non-irradiated SF_6 show a normal ratio of $^{34}S/^{32}S$ to be 0.044 ± 0.002.

5.3 Results and Discussion

Fig. 2 shows the results of the percent dissociation of the two isotopes, $^{32}SF_6$ and $^{34}SF_6$, in the neat reaction of SF_6 at various pressures from 0.1 torr to 1 torr after irradiation with 500 laser pulses.

The dissociation yield of $^{32}SF_6$ is decreased and that of $^{34}SF_6$ is slightly increased as the SF_6 pressure is increased. The results indicate, by the different trends of pressure dependence for the two isotopic species, that the energy transfer between them by collisions plays a role in this pressure regime. At a torr of SF_6, the collision frequency for an unexcited molecule calculated from simple collision theory is approximately 0.5 μs at room temperature. For the collisions including the excited molecules, the collision frequency will be higher due to the excited molecule's higher momentum. Therefore, energy transfer through bimolecular collisions by exchange reactions such as

$$^{32}SF_6^* + {}^{34}SF_6 \rightarrow {}^{32}SF_6 + {}^{34}SF_6^*$$

$$^{32}SF_6^* + {}^{34}SF_6^* \rightarrow {}^{32}SF_6 + {}^{34}SF_5 + F$$

would increase the reaction yield of $^{34}SF_6$. On the other hand, the deactivation of excited $^{32}SF_6$ molecules by these exchange reactions results in a decrease in the $^{32}SF_6$ reaction yield.

To acquire the energy from a laser beam, molecules have to be able to directly absorb laser photons at the particular laser line used. For $^{34}SF_6$ molecules, the frequency of ν_3 mode is 14 cm^{-1} away from the P(20) 10.6 CO_2 laser frequency so that the absorption efficiency on this laser line by $^{34}SF_6$ molecules is quite low. Calculated values of the dynamic stark effect for electric fields of 10^8 V/cm and are 0.1 cm^{-1} and 5 cm^{-1}, respectively[4]. The extra 10 cm^{-1} distance away from the resonant laser line would thus render $^{34}SF_6$ a significantly weaker absorber. To

obtain the laser absorption efficiencies of the two isotopes, without collisional effects, one can extrapolate the dissociation yield to zero pressure. In the low pressure regime the laser energy is absorbed by a constant fraction of reactant molecules so that a constant dissociation yield will be observed if the collisional effects can be ignored. Therefore, the deviations from this constant value are due to the collisional effects in this pressure regime. These extrapolated dissociation yields for $^{32}SF_6$ and $^{34}SF_6$ are 90% and 28%, respectively, subsequent to irradiation with 500 laser pulses of 1 μs duration each. Since these results do not include collisional effects the yields are the "unimolecular" dissociation yields for the two isotopes.

The consequence of the difference in the laser absorption efficiencies for different isotopes results in the enrichment of the less dissociated isotope in the residual sample. The enrichment factor, β, is defined as the ratio of the ratio of the concentrations of the two isotopes, $^{34}SF_6$ and $^{32}SF_6$, after to before irradiation. The ratio of $^{34}SF_6$ to $^{32}SF_6$ before irradiation is a constant, $.044 \pm .002$, the natural abundance. Thus the enrichment factor, β, is determined by the unreacted concentrations of the two isotopes after irradiation with a preset number of laser pulses. It is apparent that the enrichment factor will be a constant if the results after irradiation are determined solely by the unimolecular dissociation yields of the two isotopes. However, as the pressure is increased and the collisional effects are more pronounced, the enrichment factor decreases reflecting the decrease in dissociation yield of $^{32}SF_6$ and the increase in dissociation yield of $^{34}SF_6$. This is due to the net energy transfer from $^{32}SF_6^*$ to $^{34}SF_6$.

Laser induced dissociations require fairly high laser fluxes, usually, this high flux is obtained by focussing the laser beam into the reaction cell. Consequently, only molecules in the irradiated volume are excited by laser beam. However, even within this irradiated volume, not all the reactant molecules but only a portion of them are able to acquire sufficient energy to be dissociated. Thus, only a small fraction of reactant molecules in the cell is dissociated on each laser pulse. If we define the quantity N as the fraction of reactant molecules dissociated by a single laser pulse, the fraction of reactant molecules left in the cell after a laser pulse is equal to (1-N). It is assumed that the unreacted molecules are redistributed in the cell between two laser pulses (1 sec), so that the same fraction of reactant molecules will be dissociated for the next laser pulse without regard to the decreasing number of reactant molecules in the cell. Thus a simple relation between the fraction of reactant molecules left and the number of laser pulses can be written as

$$N_q = (1-N)^q \qquad (1)$$

where q is the number of laser pulses and N_q is the fraction of the reactant molecules left after q laser pulses. The quantity, N, is dependent on the irradiated volume, the cell volume, the sample pressure, the presence of different gases, and the various laser conditions such as laser frequency, laser intensity and is independent of the number of laser pulses.

The experimental results of the dependence of N on laser flux have been demonstrated by previous workers[5,8]. They found that fraction of $^{32}SF_6$ removed per laser pulse is proportional to the cubic power of

the laser itensity in the range from 2 to 7.2 J/cm^2 and to the fourth power in the range from .9 to 2 J/cm^2. The quantity N also varies with initial SF_6 pressure and the presence of different additional gases. In the presence of different gases and higher pressures of SF_6 the fraction dissociated per laser pulse is significantly altered by collisions between reactant molecules and foreign gas molecules. Thus, with increasing pressure, the collisional effects are more pronounced and the N shows different results.

Fig.1 is a typical IR spectra of a mixture of 1 torr SF_6 and 1 torr H_2 irradiated for preset and different number of laser pulses. The concentrations of $^{32}SF_6$ (948 cm^{-1}peak) decreases with the increasing number of laser pulses. After 3500 laser pulses the $^{32}SF_6$ peak has disappeared but there still is one-third of the original $^{34}SF_6$ left. The plots of log (Nq) of the two isotopes against the number of laser pulses are shown in Fig.3 as solid lines. The linear relationship between log Nq and q demonstrates the applicability of Eq. (1). With which we have also calculated the unimolecular dissociation yields per laser pulse for $^{32}SF_6$ and $^{34}SF_6$ from the data obtained with 500 laser pulses. These calculated unimolecular dissociation yields per laser pulse are 4.59×10^{-3} and 6.85×10^{-4} for $^{32}SF_6$ and $^{34}SF_6$, respectively. Since the ratio of irradiated volume to the cell volume in the experiments is 2.4×10^{-2}, the results imply that one-fifth of $^{32}SF_6$ and one-fortieth of $^{34}SF_6$ molecules in the irradiated volume underwent unimolecular decomposition per laser pulse under our laser conditions. From these data and Eq. (1), the fractions left of the two isotopes which underwent unimolecular decomposition at various numbers of laser pulses were calculated and shown as broken

lines in Fig. 3. It can be seen that the concentrations of the two isotopes from these calculations are decreasing much faster with increasing number of laser pulses than the corresponding experimental results shown in solid lines.

The experimental observations of SF_6 dissociation in the presence and absence of foreign collision partners are summarized in Table 1. A number of observations may be thus summarized: at a preset number of laser pulses e.g. 500, the dissociation yields for $^{32}SF_6$ and $^{34}SF_6$ are markedly affected by addition of 200 mtorr of foreign gas. The former is effectively constant (within experimental error) while the latter obviously increases. When H_2 is the collision partner the dissociation of both species drastically decreases.

As the pressure of rare gases is increased 100 fold a marked mass dependence is rather evident. The dissociation of $^{32}SF_6$ being less efficient as the mass of the collision partner decreases. The same is true of the $^{34}SF_6$ and even more dramatically demonstrated when H_2 becomes the collision partner. Lastly it should be stated that under identical conditions of pressure when the number of laser pulses is increased a gradual return to the dissociation behaviour of pure SF_6 is observed. For example compare the 98.6% of pure $^{32}SF_6$ with 1150 pulses to the 90.5% with 200 mtorr of H_2 or the 82.4% with 20.3 torr of He.

These data can be argued to fit a collisionally controlled dissociation rate which dominates the collisionless dissociation at prescribed pressure regimes and laser parameters.

While no intermolecular V-V transfer can be invoked to explain the enhanced dissociation rate of $^{34}SF_6$ at low foreign gas pressures

Table 1

Summarized results of LIS in 0.2 torr SF_6 with and without foreign gases

REACTANTS	NUMBER OF LASER PULSES	% DISSOCIATION $^{32}SF_6$	% DISSOCIATION $^{34}SF_6$	ENRICHMENT FACTOR, β
.2 T SF_6	500	89.9	40.2	5.92
	1150	98.6	48.0	38.0
	1500	----	74.1	----
+ .2 T Ar	500	90.8	48.7	5.61
+ .2 T Ne	500	91.1	44.4	6.22
+ .2 T He	500	91.9	43.2	7.01
	1000	99.1	62.8	39.7
	1500	----	61.1	----
+ .2 T H_2	500	78.2	23.5	3.51
	1000	90.5	25.0	7.89
	1500	96.3	60.0	10.7
	2000	----	72.8	----
+ 19.3 T Ar	500	81.6	44.8	3.00
+ 20.2 T Ne	500	78.8	39.1	2.87
+ 20.3 T He	500	60.0	36.2	1.60
	1000	82.4	40.7	3.37
	1500	92.3	51.3	6.32
+ 20.6 T H_2	500	42.0	15.4	1.46

V-T/R mechanism can. In particular the rotational relaxation time of SF_6 is quite rapid approximately 80 ns at 200 mtorr[9] thus implying a single or a few gas kinetic collisions per relaxation event. Thus within the duration of a laser pulse the bleached rotational levels are refilled by collisions with the rare gas molecules resulting in an increased absorption for both species. Subsequently, more efficient V-V collisional energy transfer with $^{32}SF_6$* species results in the observed higher dissociation yield for the $^{34}SF_6$ molecules. The drastic decrease of dissociation observed for both species with the addition of H_2 is a convincing demonstration of the latter species highly efficient V-T/R deactivation rate (note that at an increased number of pulses a return to the collisionless dissociation value is observed). Accepting the fact that $^{32}SF_6$ dissociates collisionlessly to an extent determined solely by the laser flux, and irradiated volume of SF_6 is it quite reasonable to ascribe the obvious increase in the dissociation of $^{34}SF_6$ to collisional effects. The collisionless dissociation of the $^{34}SF_6$ is not efficient within our experimental constraints. The added H_2 for example inhibits an originally excited $^{34}SF_6$ species from dissociation more effectively than it can inhibit a highly excited $^{32}SF_6$ from achieving dissociation. For example 200 mtorr of H_2 reduce the dissociation of the 34 species by almost a factor of two while reducing the 32 species only by 12% and so on.

These results are in total accord with the high pressure experiments in which the normal expected trend of V-T/R deactivation efficiency dependence on the reduced mass is followed; deactivation being much more efficient with the lighter mass collision-partners and consequently

lowering the dissociation rate seriously. Quite clearly the added rotational channels in H_2 contribute heavily to the total deactivation rate and reducing the percent dissociation even further.

The domination of equation(1) even in the collisionally induced LIS is still demonstrated. Since Nq, the fraction of reactant molecules left will decrease as q will increase the enrichment factor will still increase. Indeed this is born out by the data and can perhaps most clearly be seen in the case of He addition, where showed that enrichment ratios quite close to those found in pure SF_6 still be achieved in a larger number of laser pulses.

5.4 Conclusions

The experimental verification of LIS of SF_6 with and without added gases and at longer laser pulses than usually used points out some features which are in our opinion reasonably desirable in view of scale up modelling.

It is demonstrated that a number of rotational states participate in the process of collisional dissociation which follows the collisionless dissociation at lower pressures. It is shown that efficient rotational relaxation can enhance the dissociation rate. It is shown that high pressure addition of a rare gas does not preclude efficient LIS in SF_6. And finally it is shown that a measure of efficiency at specific pressure and flux conditions can still result in unneeded dissociation of the desired end product unless careful consideration to the number of puleses is given.

References

1. R. V. Ambartsumyan, Yu. A. Gorokhov, V. S. Letokhov and G. N. Makarov, JETP Lett 21, 171 (1975).

2. J. L. Lyman, R. J. Jensen, J. Rink, C. P. Robinson and S. D. Rockwood, Appl. Phys. Lett 27, 87 (1975).

3. J. Stone, M. F. Goodman and D. A. Dows, Chem. Phys. Lett 44, 411 (1976).

4. J. P. Aldridge, J. H. Birely, C. D. Cantrell and D. C. Cartwright, in Laser photochemistry, Tunable Lasers and Other Topics. Physics of Quantum Electronics Vol. 4, ed. S. F. Jacobs, M. Sargent III, M. O. Scully and C. T. Walker (Addison-Wesley, Reading, Mass.) Page 57.

5. W. Fuß and T. P. Cotter, Appl. Phys. 12, 265 (1977).

6. J. G. Black, E. Yablonovitch, N. Bloembergen and S. Mukamel, Phys. Rev. Lett 38, 1131 (1977).

7. H. Brunet and M. Perez, J. Mol. Spectrosc. 29, 472 (1969).

8. J. D. Campbell, G. Hancock and K. H. Welge, Chem. Phys. Lett 43, 581 (1976).

9. J. L. Lyman and S. D. Rockwood, J. Appl. Phys. 47, 595 (1976).

Figures Caption

Figure 1. The IR spectra of a mixture of 1 torr SF_6 and 1 torr H_2 irradiated for preset and different numbers of laser pulses.

Figure 2. Percent dissociation of the two isotopes, $^{32}SF_6$ and $^{34}SF_6$, in the neat reaction of SF_6 at various pressures from 0.1 torr to 1 torr after irradiation with 500 laser pulses.

Figure 3. Plots of $\log(N_q)$ of the two isotopes species vs. the number of laser pulses for a mixture of 1 torr SF_6 and 1 torr H_2. Solid lines are experimental results. Broken lines indicate calculated unimolecular dissociation, see text of equation (1).

Figure 1

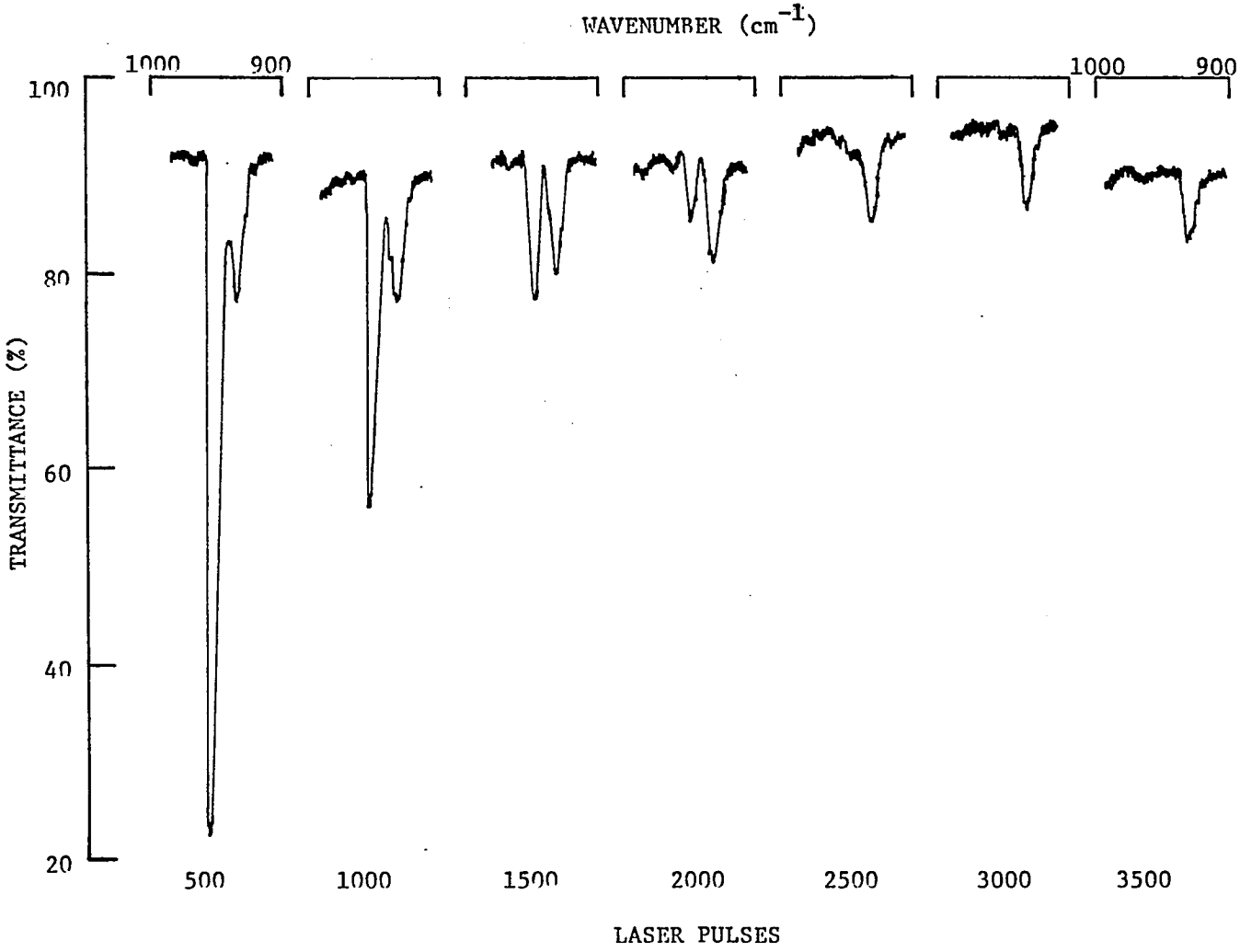
WAVENUMBER (cm^{-1})
1000
900
1000
900
100
80
60
40
20
TRANSMITTANCE (%)
500
1000
1500
2000
2500
3000
3500
LASER PULSES

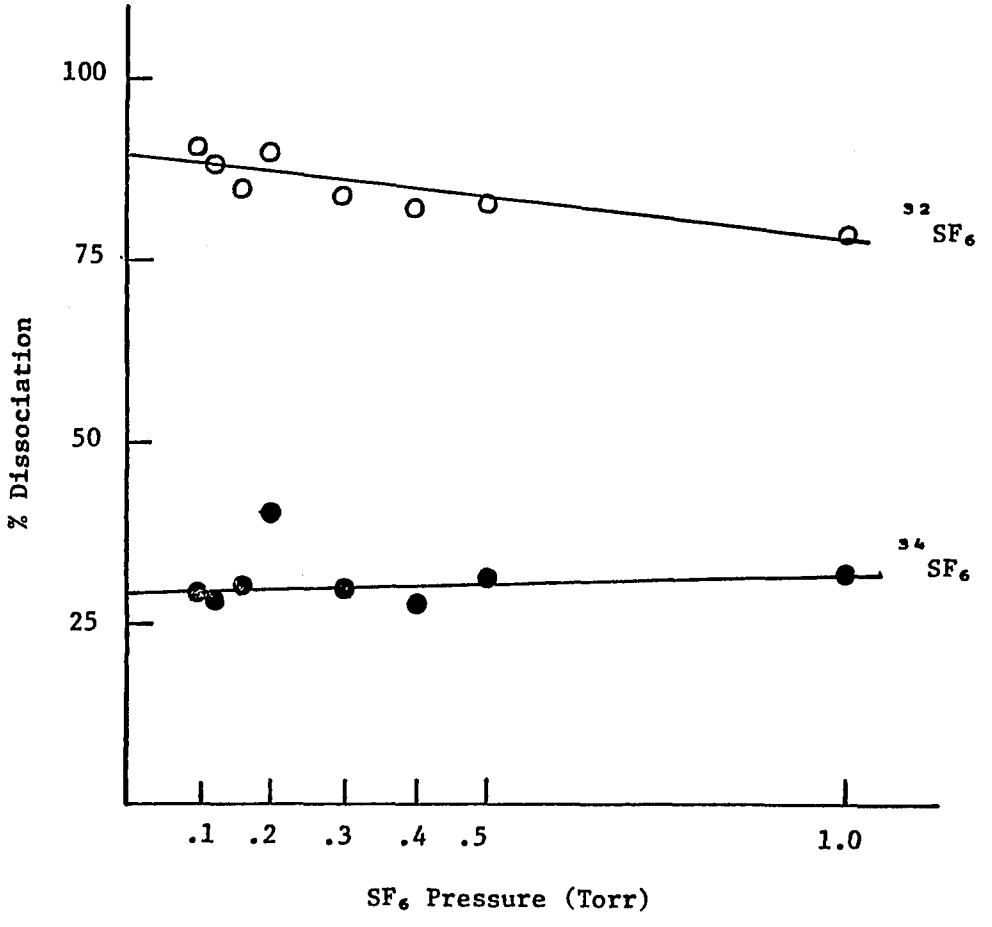
100
75
50
25
% Dissociation
32 SF6
34 SF6
.1
.2
.3
.4
.5
1.0
SF6 Pressure (Torr)

Figure 2

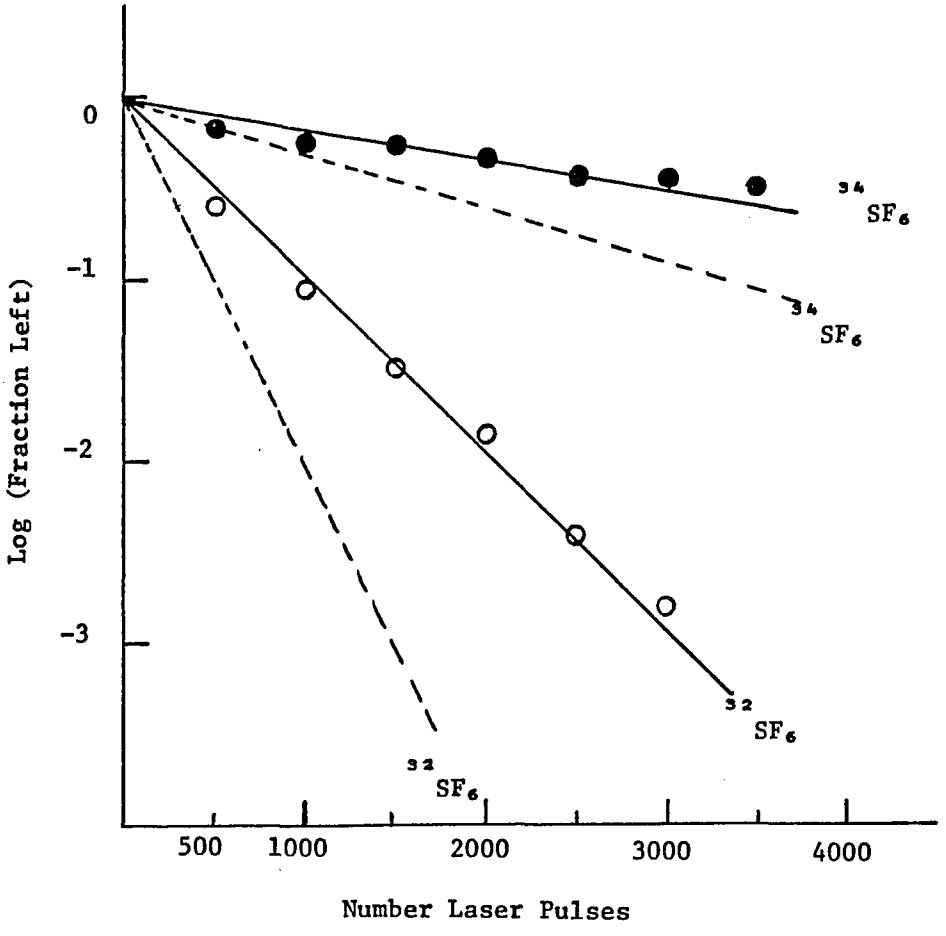
0
-1
-2
-3
Log (Fraction Left)
500
1000
2000
3000
4000
Number Laser Pulses
34 SF6
34 SF6
32 SF6
32 SF6

Figure 3

Chapter 6

LASER INDUCED CHEMICAL REACTIONS IN SF_6

6.1 Introduction

Multiphoton laser induced reactions of SF_6 in the neat and with hydrogen mixtures are reported on in this chapter. The copious formation of suspended particulates is particularly interesting since it supports the predominant mechanism in high temperature reactions. This particular species, SF_6, has been the subject of a large number of investigations all predicated on multiphoton dissociation with IR lasers. No reports of sulfur formation has been given previously. It has long been argued that chemical reaction induced by infrared lasers produce nonequilibrium populations of particular degrees of freedom. These are deemed responsible for the different operational mechanisms from thermally driven reactions and thus leading to different product formation[1]. Experimental results obtained with various compounds in our laboratory[2,3], in addition to other work[4,5], strongly indicate that the reaction pathway is always associated with the lowest thermal dissociation channel(s) of the excited molecule. Recently a theoretical model based on statistical thermodynamical process has been proposed to account for collisionless multiphoton dissociation[6]. The particulate formation found in this reaction at different pressure regimes suggests further to support the essentially statistical behavior of laser induced chemical reactions.

6.2 Experimental

The detailed laser setup was identical to that described in Chapter 5. SF_6 and H_2 were Matheson research grade and used without further purification.

Product analysis was carried out by infrared spectroscopy (Perkin-Elmer Model 267) and mass spectrometer (Varian CH-7). Product and reactant peaks were compared prior to and subsequent to laser irradiation for a preset number of shots at predetermined frequencies and 2J of output power. The beam was either used directly or focussed with a 5 inch focal length ZnSe lens. Pulse lengths of 300 ns FWHM and ~700 tail were used throughout. The repetition rates were typically 50 pulses per minute.

6.3 Results

6.3.1 Reaction of SF_6 in the neat

The CO_2 laser radiation at 944.15 cm^{-1} corresponding to the P(20) 10.6μ is strongly absorbed by SF_6 (ν_3) vibrational mode. At pressures above 40 torr and with input power of 2J the laser beam is not detectable after passing through a 10 cm sample cell indicating that all photons are absorbed. Such a strong absorption efficiency by SF_6 at this wavelength leads to the observation of unimolecular dissociation of SF_6 at low pressures. A blue fluorescence emission is always visible in the pressure range studied, the intensity of fluorescence increases

with the SF_6 pressure and consequently is gradually reduced pulse by pulse corresponding to the decrease in SF_6 pressure in the reaction cell. The origin of this fluorescence may well depend on particular fragmentation and subsequent recombinations. Further, since particulates of S were identified as a final product the possibility of detection of early nucleation was investigated by light scattering techniques using a 0.5 mW He-Ne laser. A He-Ne laser beam was directed through the cell at right angles to the CO_2 laser beam. During the laser pulse and at pressures above 20 torr, some reflected points were observed due to the scattering of the He-Ne beam by the particles produced. However, although these particles were observed during a laser pulse, no particulates observed subsequent to laser pulse termination. The He-Ne laser with its output wavelength at 6328 Å can in principle allow efficient scattering from particles no smaller than 60 Å. The reflected points observed during the laser pulses indicate that the particles formed were at least several tens of sulfur atoms aggregated at same particular morphology. However, the recombination process of S and F is very efficient and competes very effectly with S, S recombinations thus little or no solid sulfur can be detected after the laser pulse has been cut off.

The detectable products in this reaction were SOF_2, SiF_4, CF_4, SOF_4 and SF_4 as determined by infrared and mass spectral analysis after irradiation with 1000 focussed laser pulses. At pressures exceeding 80 torr SO_2F_2 and COF_2 were also observable. Formation of CF_4 and COF_2 were due to the fluorine atom attack on the O-ring and vacuum grease since black circles were observed on the entrance window at the contact points of the O-ring with window in most of the observed cases. SiF_4

was formed by the reaction

$$4F + SiO_2(glass) \longrightarrow SiF_4 + 2O \qquad (1)$$

where the initial F atom appears from $SF_6 \longrightarrow SF_5 + F$. With an unfocussed laser beam, reaction at 80 torr was also induced with the observation of the fluorescence at the entrance window and the nearly identical products SOF_2, SiF_4 and traces of CF_4.

The reactions induced with P(20) 9.6μ laser line, corresponding to the 1046.85 cm^{-1}, were also studied. Since this frequency does not correspond to any vibrational frequency of SF_6 the reaction can only be induced by gas breakdown which occurs under fixed laser pulse conditions above a threshold pressure of SF_6. The threshold pressure of SF_6 under the laser conditions used in this study was 20 torr. Product formation was found to be the same as that obtained with the resonant irradiation (P(20) 10.6μ).

6.3.2 Reactions of SF_6 with H_2

This reaction was investigated over the pressure range of 20-160 torr. The ratio of SF_6:H_2 was held to 1:1. Irradiation with the resonant P(20) 10.6μ at various pressures revealed the common products SiF_4, SO_2, SOF_2, SO_2F_2, HCl and CF_4. When 160 torr of sample was irradiated with an unfocussed laser beam, SOF_2 and SiF_4 were the only products. The visible emission in this particular case was stronger at the entrance window to the cell and gradually diminished and finally

disappeared after traversing a 2 cm path. Formation of HCl due to the reaction of Cl atom, which was released from NaCl window by the fluorine atoms, with H_2. The formation of CF_4 is very small indicating that F atoms were efficiently scavenged by H_2 to form HF which immediately reacts with the glass walls leading to the formation of SiF_4 as a major product.

The visible blue fluorescence was the same as the reaction of SF_6 in the neat. The obvious difference is the copious particulate formation in this reaction. The particulates were always observed in this pressure range. At total pressures below 100 torr, the particulates were formed and eventually deposited isotropically throughout the cell. These aggregated particulates of sulfur were so small as to remain suspended for observable times (seconds). However, at pressures exceeding 100 torr, very thick particulates were deposited on the wall extending from directly behind the entrance window to the focussing point. Beyond the focussing point the particulates were not visible. The particulates formed in this pressure regime are so large that they were observed to fall towards the cell walls very quickly. From these rather crude observations it is nevertheless clear that there exist two very different sizes of particulates in the two pressure regimes. Thus, their creation must involve different nucleation times. In order to establish the nucleation times corresponding to these different sizes of particulates the following experiment was performed. An attenuated He-Ne beam was directed to pass through the cell at right angles of the CO_2 laser beam and a phototube was seated on the other side of cell to receive the signal. The beam intersection point was about the half way

between entrance window and the focal point. A 6328 Å bandpass filter was inserted between cell and phototube such that the phototube is only sensitive to the red He-Ne beam. The signal was triggered by the laser pulse and displayed on a oscilloscope. When the particulates were formed in the He-Ne beam, the intensity of the beam was reduced and the nucleation time is defined as the time delay between the laser pulse and the phototube signal reduction. The nucleation times for the pressures at 100 and 160 torr were measured as 60 and 100 μs, respectively.

To estimate the size of the particulates, a larger cell was used for a modified Millikan oil drop experiment. The velocity of the falling particulate was measured by clocking the time for the particulate to traverse a known distance between two points. Applying Stokes' law, the equation[12] reads

$$\frac{4}{3}\pi r^3 (\rho - \rho_o) g = 6\pi\eta r \left(\frac{dx}{dt}\right) \qquad (2)$$

where

r = radius of sphere,

ρ = density of sphere,

ρ_o = density of medium,

g = acceleration of gravity,

η = coefficient of viscosity of the gas,

$\frac{dx}{dt}$ = velocity of the falling sphere,

the coefficient of viscosity of the gas is given by

$$\eta = \frac{5}{16}\frac{(\pi\, m\, k\, T)^{1/2}}{\pi\,\sigma^2}$$

$$= 2.67 \times 10^{-5}\,(M\,T)^{\frac{1}{2}}/\sigma^2,\ g\ cm^{-1}sec^{-1} \qquad (3)$$

where

M = molecular weight,

T = temperature in ^{o}K,

σ = molecular diameter in $\mathring{A}$.

At 100 torr, the size of the particulates was measured to be approximately 2 μm as calculated via equation (2) for a distance of 8.2 cm defined by a two laser beams and an elapsed time of 129 sec.

Sulfur particulates were also analyzed by X-ray diffraction method. The results indicate that sulfur particulates formed from low pressure samples of SF_6/H_2 mixtures were completely amorphous. High pressure samples (i.e., larger than 100 torr) show a majority of amorphous sulfur but a small concentration of crystallites.

The threshold pressure to induce a gas breakdown with the non-resonant P(20) 9.6μ laser line was approximately 20 torr. The particulates were formed and deposited solely around the focal point. Product analysis showed the identical results as in the on resonance cases at equivalent pressures.

6.4 Discussion

With a high intensity infrared CO_2 laser, the primary step is the dissociation of SF_6 into SF_5 and F.[7] The SF_5 radical is not stable

and further decomposes, either directly or aided by the laser radiation, into SF_4 and an additional F. However, SF_4 is an extremely reactive substance toward moisture so as to be instantly hydrolyzed to form SOF_2.[8] Formation of SOF_4 is undoubtedly taking place via highly vibrationally excited SF_4 and an oxygen atom released from reaction of fluorine atom with the glass (SiO_2) as shown in equation(1). Another mechanism to form SOF_4 may be due to the recombination of SOF_2 and F since both are in fair abundance.

In the presence of H_2 the products are different, SO_2F_2 and SO_2 predominate instead of the SOF_4. This particular channel is heavily favored if water is formed or is present in the cell since SOF_4 reacts very rigorously with water producing SO_2F_2.[8] The latter also hydrolyzes vigorously to form SO_2. All the products can be easily accounted for by well known thermal reaction pathways, however, the sulfur formation is somewhat different.

Sulfur has been observed by electrical decomposition of SF_6[9] and by nonresonant microwave excitation of SF_4[10]. In the former case, reaction pathways were postulated as

$$SF_5^+ + SF_5^- \longrightarrow (S_2F_{10})^*$$

$$(S_2F_{10})^* \longrightarrow S_2F_2 + 8F$$

$$S_2F_2 \longrightarrow SF_2 + [S]$$

The reaction involved ionic species due to gas breakdown when discharged. Thermal decomposition of S_2F_2 led to the final products of SF_2 and sulfur. This seems not to be applicable to our experiments since no

SF_2 was formed in our results although the mechanisms of off resonance also went through gas breakdown and the ions were formed at the focal region. To account for the formation of sulfur from SF_4, it was postulated that under microwave excitation SF_4 completely disproportionated to sulfur and fluorine atoms subsequent recombinations outside the high field zone yield SF_6. S_2F_{10} was examined by the same authors the results showed the same products SF_6 and sulfur. The authors agreed that since the discharge intensity is so high that atomic species dominated, recombination resulted in the most stable products namely SF_6 and sulfur.

In the P(20) 9.6μ nonresonant gas breakdown experiments in the absence of H_2, the atomic species are dominant inside the plasma. We thus expected that sulfur and fluorine atoms be the preferred species in such a high temperature zone. Lack of thermodynamic data for SF_4, S_2F_2, SF_2 and F precludes calculation of the free energy at expected temperature of ~1500 ^{o}K. However, due to large positive entropy and positive enthalpy of sulfur at room temperature (SF_6 and SF_4 have very large negative enthalpy at room temperature, -289 and -172 Kcal/mole, respectively), it seems to be reasonable to prefer sulfur and fluorine atoms at such a high temperature. An additional and fairly conclusive piece of evidence to support this point of view was the observation of particulates during the laser pulse in the resonant process and nonresonant cases. In addition, the blue fluorescence observed in the resonant multiphoton case may be due to the formation of S_2 since the electronic absorption bands of S_2 in the visible region are well matched with the deep blue color of hot sulfur vapor. Recombination process

after dissociation of SF_6 has been recently reported however no formation of sulfur was mentioned[11].

The complete dissociation of SF_6 to form sulfur was more clearly visible when H_2 was added as a scavenger. Since the fluorine atoms were efficiently removed by hydrogen atoms (or molecules), therefore, the sulfur particulates were much more readily observed. Also the size of the particulates was observed to increase with pressure. It is thus believed that the reactions of SF_6, either with or without H_2, initiated by laser radiation occurred in two different stages. Inside the irradiation volume the SF_6 molecules were completely dissociated, subsequent recombination processes produced highly excited species and followed thermodynamically controlled final products.

The different nucleation times observed at two different pressures are consistent with homogeneous three body collisional nucleation. If the density of the formation of sulfur atoms is so high that, as soon as the initial seeds are formed, the sulfur diffuses to the neighbor seed, also if the"sticking coefficient" is very high then the size of the particulates will depend on the available number of sulfur atoms. At low pressures of reactants the density of sulfur produced is also low so that the size of the particulates is small corresponding to a shorter nucleation time. At high initial pressures of reactants the available sulfur produced is high and the size of the particulates is also large so a longer nucleation time is observed.

6.5 Conclusions

Formation of sulfur particulates was studied with CO_2 TEA laser radiation of SF_6 and SF_6/H_2 mixtures. Both multiphoton absorption processes and gas breakdown experiments were carried out at pressure ranges of 10-160 torr. It was concluded that S and F recombination processes are so fast that without an efficient scavenger sulfur particulates were not formed at sufficient density to induce light scattering of a probing He-Ne beam. Particulate formation may imply that the product formation other than sulfur occurred as the secondary process after recombination of the fragments produced in the primary stage. The presence of major products such as SF_4, SOF_2, SO_2F_2 and SOF_4 can be argued by conventional, thermodynamically controlled reaction dynamics. However, at very high fluence of the exciting CO_2 radiation SF_6 shows total decomposition to sulfur and fluorine atoms. Under these conditions the mechanisms operating in resonant multiphoton absorption and gas breakdown are essentially identical.

References

1. N. G. Basov, A. N. Oraevsky and A. V. Pankratov, Chemical and Biochemical Application of Lasers, Vol.1, C. B. Moore, ED., Academic Press, New York, 1974.

2. B. L. Earl and A. M. Ronn, Chem. Phys. Lett. 41, 29 (1976).

3. S. T. Lin and A. M. Ronn, Chem. Phys. Lett. 49, 255 (1977).

4. W. Braun and W. Tsang, Chem. Phys. Lett. 44, 354 (1976).

5. D. F. Dever and E. Grunwald, J. Am. Chem. Soc. 98, 5055 (1976).

6. J. G. Black, E. Yablonovitch, N. Bloembergen and S. Mukamel, Phys. Rev. Lett. 38, 1131 (1977).

7. M. J. Coggiola, P. A. Schulz, Y. T. Lee and Y. R. Shen, Phys. Rev. Lett. 38, 17 (1977).

8. R. D. W. Kemmitt and D. W. A. Sharp, Advances in Fluorine Chemistry, Vol. 4, M. Stacey, J. C. Tatlow and A. G. Sharpe, Eds., Butterworths, London, 1965.

9. D. Edelson, C. A. Bieling and G. T. Kohman, Ind. Eng. Chem. 45, 2094 (1953).

10. W. S. Smith and V. A. Engelhardt, J. Am. Chem. Soc. 82, 3838 (1960).

11. D. Tal, U. P. Oppenheim, G. Koven and M. Okon, Chem. Phys. Lett. 48, 67 (1977).

12. F. Daniels and R. A. Albertz, Physical Chemistry, 3rd Ed., John wiley & Sons, Inc., New York, 1967.

Chapter 7

LASER INDUCED CHEMICAL REACTIONS OF CH_2F_2

7.1 Introduction

Laser enhanced or laser induced chemical reactions constitute one of the most significant scientific developments in recent years[1-3]. While most of the limelight was captured by a number of stirkingly successful isotope separation experiments in a variety of molecular and atomic species, there remains a wealth of chemical reactions to be explored and exploited utilizing these techniques[4].

Although the number of potentially interesting reactions is literally unlimited this chapter deals with the reactions of difluoromethane. The particular interest in CH_2F_2 was generated subsequent to similar work on laser driven methyl halide reactions that were explored in detail at this laboratory[5]. The latter were originally chosen for investigation for their simplicity and thorough knowledge of the kinetic routes followed by excited species during energy transferring collisions[6].

The multiphoton laser induced reactions of the methyl halides either in the neat or with chlorine generated a number of conclusions which in turn demanded further exploration in similar yet less symmetric molecules. It was thus that the reactions of difluoromethane with chlorine and in the neat were chosen for study with a specific focus on the off resonance behavior, the efficiency in terms of photon utilization to molecules reacted, the threshold to these reactions and the particular

mechanism or mechanisms responsible for product formation.

The oxidation reaction of CH_2F_2 was also studied. It was found the reaction to be an explosive one under appropriate conditions. This chain reaction induced by an infrared laser is particularly interesting in comparison with the conventional thermal process, for potential uses in industrial processes. That is so since the ratio of the photon utilized to the molecules dissociated is very high as the result of almost complete decomposition of CH_2F_2 with a single laser pulse. In addition, the product formation of this reaction showed a different distribution depending on the sizes of the reaction cell used. The products of the decomposition (C_2F_4), primary oxidation(COF_2) and further oxidation(CO and CO_2) were found to parallel the thermal oxidation of C_2F_4 in oxygen from low to high temperatures[7-8].

7.2 Experimental

The laser apparatus was the same as described in Chapter 4. Glass cells with three different sizes, 18 cm^3 small cell, 94 cm^3 square cell and 500 cm^3 large cell fitted with NaCl windows have been used in these experiments. The laser beam was either used directly or focussed so as to fix the focal point at the center of the cells. Gases were Matheson research grade and used without further purification save for freeze thaw cycles.

Product analysis was carried out utilizing Perkin-Elmer Model 267 infrared spectrometer and Varian CH7 mass spectrometer. Product and reactant peaks were compared prior to and subsequent to laser excitation

of CH_2F_2 for a preset number of laser pulses at predetermined frequencies and power levels.

7.3 Results

7.3.1 Reactions of CH_2F_2 in the neat

The reactions of CH_2F_2 in the neat were investigated over the pressure range of 300 mtorr to 20 torr under the conditions of varying laser energies, laser frequencies and the number of laser pulses. The results are shown in Table 1. At the pressure of 300 mtorr no product is detectable with the highest attainable power level of perhaps 200-300 MW/cm^2 and an unusually large number of laser pulses when R(18)9.6μ CO_2 laser line ($1077cm^{-1}$) was used. Such a large number of laser pulses for reaction in the large cell, which contains more reactant molecules proportional to the volume ratio to the small cell, is necessary for comparison since the ratio of irradiation volume to the cell volume for the large cell is far less than that for the small cell. However, even with such a large number of laser pulses, there was no detectable product. This indicates that the reaction would not proceed as a collisionless unimolecular decomposition. This may be due to the fact that the CH_2F_2 molecule has low absorption efficiency at this laser frequency and posesses a low density of energy levels at higher total energies. At higher pressures, the reaction was not induced with an unfocussed laser beam, corresponding to the power level of ~ 3 MW/cm^2, either in the small or large cells. Therefore, in addition to the collisional excitation, a threshold

TABLE 1

The results of laser induced reactions of CH_2F_2 in the neat under various conditions

Excitation source	Pressure (torr)	Laser pulses	Products	Conditions
R(18)9.6μ	.3	4000	Not detectable	Focussed, Large cell
	3	4000	Not detectable	Unfocussed, Large cell
	3	4000	C_2F_4, SiF_4, C_2H_2	Focussed, Large cell
	3	1200	Not detectable	Unfocussed, Small cell
	3	100	C_2F_4, SiF_4	Focussed, Small cell
	3	600	C_2F_4, SiF_4, C_2H_2	Focussed, Small cell
	3	1200	C_2F_4, SiF_4, C_2H_2	Focussed, Small cell
R(34)9.6μ	3	1200	C_2F_4, SiF_4, C_2H_2	Focussed, Small cell
P(20)9.6μ	3	1200	C_2F_4, SiF_4, C_2H_2	Focussed, Small cell
	20	5	Particulates, C_2F_4, SiF_4	Focussed, Small cell
	20	100	Particulates, C_2F_4, SiF_4 C_2H_2, fluorinated olefins	Focussed, Small cell
	20	2000	SiF_4	Focussed, Small cell
P(20)10.6μ	10	1000	Not detectable	Focussed, Small cell
	20	50	Particulates, C_2F_4, SiF_4, C_2H_2	Focussed, Small cell

power level is needed to induce the reaction.

At the pressures above 3 torr the reaction was induced with a focussed beam. Weak fluorescence on each laser pulse could be observed due to the relaxation of the electronically excited fragments. The major product was C_2F_4 accompanied by a significant amount of SiF_4 from the reaction of the produced fluorinated radicals with the glass cell. C_2H_2 also became detectable with increased number of laser pulses. At pressures higher than 10 torr, some fluorinated olefins and particulates were also formed in addition to C_2F_4, SiF_4 and C_2H_2. The well-shaped orange fluorescence was produced during a laser pulse and dark brown particulates deposited all over the cell wall. The particulates were identified as carbon.

Fig.1 presents a reproduction of the infrared spectrum of pure CH_2F_2 at 10 torr in the small cell as a function of laser pulses at the resonance frequency of the R(18)9.6μ CO_2 laser line. It shows clearly the production of C_2F_4 which peaks at approximately 200 pulses. Subsequently the disappearance of the C_2F_4 and the parent peaks, the predominance of SiF_4 is very clear at 2000 pulses. Therefore, SiF_4 becomes the only product that survives in the gas phase. It should be noted that no formation of C_2H_4 or the mixed fluorine hydrogen dimer $C_2H_4F_2$ were detected while C_2F_4 dominated. Thus, the existence of the CF_2 diradical was strongly implied as evidenced by the copious formation of C_2F_4. This was further substantiated by scavenging with oxygen with a consequent formation of COF_2 as the major product as will be shown later. The formation of CF_2 diradical during the laser pulse can be attributed to the reactions

$$CH_2F_2 \xrightarrow{nh\nu} CHF_2^* + H \qquad (1)$$

$$CHF_2^* \longrightarrow CF_2^* + H \qquad (2)$$

The formation of C_2H_2 and particulates at high pressure was expected since both the C_2 and CH species have been traditionally detected in the decomposition and oxidation reactions of hydrocarbons at high temperature[9]. However, the excitation mechanisms responsible for the formation of C_2 and CH are still not totally understood[12].

Products were also observable when the laser was tuned away from the resonance line by 10 cm^{-1} to the R(34)9.6μ line (1087cm^{-1}) as well as 30 cm^{-1} to the P(20)9.6μ transition (1047cm^{-1}). No strong dependence of product concentration or nature on the laser frequency within the boundaries listed above was detected. However, a 130 cm^{-1} offset resulted in no reaction under the threshold pressure to the occurrence of dielectric breakdown. The threshold pressure at the laser power of 3J is approximately 20 torr for breakdown. The identified products were identical to those found with on resonance multiphoton absorption experiments.

7.3.2 Reactions of CH_2F_2 with Cl_2

As this investigation closely paralleled the methyl halide work mentioned previously, experimental conditions were chosen so as to compare both sets of data in the interest of establishing similar or dissimilar trends. A concise review of the methyl halide-chlorine reactions is thus included below to facilitate comparison.

The direct excitation of the C-F stretching mode in CH_3F with

the P(20)9.6μ CO_2 laser line resulted in reactions depicted schematically below.

$$CH_3F^* + Cl_2 \longrightarrow CH_2ClF + HCl$$

It was shown that the mechanism was not a radical mechanism but rather followed one or two preferred paths

$$\text{(i)}\quad CH_3F^* + Cl_2 \longrightarrow CH_3F + 2Cl.$$
$$Cl. + CH_3F \longrightarrow CH_2FCl + H.$$

or

$$\text{(ii)}\quad CH_3F^* + Cl_2 \longrightarrow Cl_2 + CH_2F. + H.$$
$$Cl_2 + H. \longrightarrow HCl + Cl.$$
$$Cl. + CH_2F. \longrightarrow CH_2FCl$$

The reaction product was limited to CH_2FCl when the CH_3F/Cl_2 ratio was held at 1:1 and successive chlorination occurred as the ratio increased in favor of chlorine. Off resonant pumping up to $\pm$ 50 cm^{-1} of the known absorption in CH_3F yielded significant and identical products. Finally it was shown that no product formation was detectable when the laser power level was less than 100 MW/cm^2. At this and higher powers conversion efficiency was at best 20% of initial reactants. No dimerization reaction of the neat CH_3F (or other halides) were observed and products were identical at pressures ranging from 200 mtorr to 60 torr of CH_3F and Cl_2 in the bimolecular case. The speculation then regarding the nature of the operating mechanism was that either (i) or (ii) or both were operative and that the large off resonance behavior was due to the very high level density generated by the very high electric field (275 KV/cm) of the high power laser.

Thus a prior set of hypotheses existed before the investi-

gations of CH_2F_2 began. It was conjectured that the reaction (3a) will predominate over (3b) as it did in the CH_3F case despite the fact that the C-F vibration

$$CH_2F_2 + Cl_2 \longrightarrow CHF_2Cl + HCl \quad \Delta H = -27\ ^{Kcal}/_{mole} \qquad (3a)$$

$$CH_2F_2 + Cl_2 \longrightarrow CH_2FCl + FCl \quad \Delta H = +32\ ^{Kcal}/_{mole} \qquad (3b)$$

was laser driven in both cases.

Off resonant behaviour was anticipated to be somewhat more restrictive since no first order mixing was possible with the C_{2v} symmetry of the difluoromethane. Additionally, the threshold power for initiation was expected to be lower since the addition of a fluorine weakens the carbon hydrogen bond significantly (~23 Kcal)[13]. The experimental results presented below essentially follow all the anticipated trends. Table 2 shows the data taken with samples of ranging from 2 torr to 12 torr at different ratios of reactants. Excitation was provided on the resonant R(18)9.6μ CO_2 laser line and products were analysed for by mass and infrared spectroscopy and the listings of products are from left to right in order of decreasing abundance.

The results obtained from the reactions of CH_2F_2 in the neat, as shown in the above section, show C_2F_4 was the major product. In the presence of Cl_2, however, the dimerization depends on the scavenger ratio in the mixture. At 1:4 ratios high in Cl_2, no dimerization was observed at all. No formation of SiF_4 was detected either. In high CH_2F_2 ratios, product formation showed no dependence on the number of the laser pulses, only the singly chlorinated species CHF_2Cl was detected along with the products detected in the neat reaction. At a 1:1 ratio, no product was detected when an unfocussed beam was used. Note

TABLE 2

The product distribution of reactions of CH_2F_2 with Cl_2 at various pressures of different reactants ratio obtained by irradiation with R(18)9.6μ CO_2 laser line at power energy of 1J

Total pressure (torr)	CH_2F_2/Cl_2 ratio	Laser pulses	Products	Conditions
6	5:1	300	C_2F_4, CHF_2Cl, SiF_4	Focussed, Small cell
	5:1	1200	C_2F_4, CHF_2Cl, SiF_4	Focussed, Small cell
	4:1	600	C_2F_4, CHF_2Cl, SiF_4	Focussed, Small cell
3	2:1	1200	C_2F_4, CHF_2Cl, SiF_4	Focussed, Small cell
6	1:1	1200	Not detectable	Unfocussed, Small cell
	1:1	1200	C_2F_4, CHF_2Cl, SiF_4	Focussed, Small cell
2	1:4	1350	CHF_2Cl	Focussed, Large cell
10	1:4	1200	CHF_2Cl, $C_2F_4Cl_2$, CF_2Cl_2	Focussed, Large cell
	1:4	6200	CHF_2Cl, CF_2Cl_2, $C_2F_4Cl_2$	Focussed, Large cell
	1:4	1200	$C_2F_4Cl_2$, CF_2Cl_2, CHF_2Cl	Focussed, Small cell
12	1:5	5	CHF_2Cl	Focussed, Small cell
	1:5	100	CHF_2Cl, CF_2Cl_2, $C_2F_4Cl_2$	Focussed, Small cell
	1:5	4500	$C_2F_4Cl_2$, CF_2Cl_2, CHF_2Cl	Focussed, Small cell

TABLE 2 (continued)

Total pressure (torr)	CH_2F_2/Cl_2 ratio	Laser pulses	Products	Conditions
	1:5	1200	CHF_2Cl	Unfocussed, Small cell
	1:5	1200	CHF_2Cl, CF_2Cl_2, $C_2F_4Cl_2$	Unfocussed, Large cell
		4500	CHF_2Cl, CF_2Cl_2, $C_2F_4Cl_2$	Unfocussed, Large cell

that in experiments with high chlorine ratio, the reaction to form CHF_2Cl is clearly very efficient as product formation is very obvious after 5 laser pulses. No geometric power threshold is obvious since the reaction is driven in the unfocussed geometry towards the single product. It was attempted to drive the reaction with a lower power Q-switch laser, however, no product formation was detectable at power levels of 10KW.

It was also found that multiple chlorination proceeds as a function of laser pulses. The doubly chlorinated species along with $C_2F_4Cl_2$ were detected after 100 laser pulses. However, no triply or totally chlorinated species were observed. New product, $C_2F_4Cl_2$, appears at 100 pulses at low concentration and dominates at a high number of pulses. The implication being that the initial product CHF_2Cl rereacts subsequently to its formation via either direct laser excitation or via collisions with collisionally excited CH_2F_2 molecules (one of the vibrational frequencies of CHF_2Cl is nearly matched with that of CH_2F_2 and is very close to the R(18)9.6μ CO_2 laser line[14]). The existence of a $CF_2Cl\cdot$ radical is certainly suggestible at this point since its dimer becomes a major product at long excitation times.

7.3.3 Reactions of CH_2F_2 with O_2

The laser induced oxidation reaction of CH_2F_2 driven at three different frequencies of infrared photons was also studied. Under appropriate conditions, this oxidation reaction was found to be explosive. Since no such a thermal reaction was reported previously, the result was particularly interesting, since two distinct electronic emission bands

were observed as cell conditions were varied. This may imply that two different mechanistic routes were involved in this chain reaction each depending on the dominant propagators produced by branching chains. The results at various conditions of excitation sources, reactants' ratio, total pressure, size of the reaction cell and conditions of the reaction cell are shown in Table 3.

As pointed out previously, there is no difference in product formation utilizing either the R(18) or P(20) 9.6μ CO_2 laser lines as excitation sources under the same conditions. The threshold pressure must be increased when the laser frequency was further tuned away to P(20)10.6μ laser line from the resonant frequency of the CH_2F_2 molecule. This is expected since neither the oxygen molecule, similar to the chlorine molecule described in the last section, nor the CH_2F_2 molecule shows resonant absorption at this frequency. Therefore, more reactant molecules are needed to interact with photons and/or to have more collisions between reactant molecules so as to induce the reaction at limited energy thresholds. It was also shown that products containing CH bond were not observed at all. However, C_2F_4 was still observed both at a 1:1 ratio under the threshold pressure of the explosion limit and at the ratios high in CH_2F_2. The former information indicates that the processes of association of radicals which is responsible for the formation of C_2H_2 in the neat reaction can not be important in the presence of oxygen. The latter result is further evidence of the large abundance of CF_2 diradicals in the neat reactions.

According to the reactants' ratio, the results are outlined as follows

TABLE 3

The results of the reactions of CH_2F_2 with O_2 obtained by irradiation with a focussed CO_2 laser beam.

Excitation source	CH_2F_2/O_2 ratio	Total pressure (torr)	Laser pulses	Products [a]	Conditions [b]
R(18)9.6μ	1:10	22	200	COF_2	Small cell
	1:9	60	200	COF_2	Small cell
	4:1	25	200	COF_2, C_2F_4	Small cell
	1:1	12	200	COF_2, C_2F_4	Small cell
		20	100	COF_2	Small cell
		20	1	COF_2	Conditioned small cell, Orange explosion
	3:1	20	200	COF_2	Large cell
	5:1	9	500	COF_2	Large cell
	1:1	20	1	CO, CO_2	Large cell, Green explosion
		20	1	CO, CO_2	Conditioned large cell, Orange explosion
		20	1	CO, CO_2, COF_2	Large cell with surface tripled, Green explosion

TABLE 3 (continued)

Excitation source	CH_2F_2/O_2 ratio	Total pressure (torr)	Laser pulses	Products[a]	Conditions[b]
P(20)9.6μ	1:1	20	100	COF_2	Small cell
		20	1	CO, CO_2	Conditioned Large cell, orange explosion
P(20)10.6μ	1:1	60	100	Not detectable	Small cell
		40	1	CO, CO_2	Large cell, Green explosion

(a) SiF_4 was the common product for all reactions. Particulates (fine crystals) were also found on the wall of reaction cell after explosion.

(b) The output power of laser beam was 1.5 J for R(18) 9.6μ line and 2.5 J for P(20) of either the 9.6μ or the 10.6μ lines.

(A) High O_2: CH_2F_2 ratio : Experiments were only performed in the small cell. The results shown in Table 3 point out that COF_2 was the only product even at pressure as high as 60 torr. This exclusive production of COF_2 strongly indicates that the reaction pathways follow equations (4) and (5)

$$CHF_2^* + O_2 \longrightarrow COF_2 + OH \qquad (4)$$

$$CF_2^* + O_2 \longrightarrow COF_2 + O \qquad (5)$$

The process

$$CH_2F_2^* + O_2 \longrightarrow COF_2 + H_2O \qquad (6)$$

is not favorable since O_2 molecule would act as an efficient quenching agent rather than a reacting species to form COF_2 due to the fact that the process requires two bonds to be ruptured, consequently, other products such as CHFO would be observed. The process of recombination of CF_2 diradicals becomes statistically unfavorable at high ratios of O_2 to CH_2F_2 pressures, however, the complete oxidation products namely CO and CO_2 were not found. Therefore, the cell wall may be functioning as an effective deactivator to quench further oxidation reactions.

(B) High in CH_2F_2 ratio : Reactions were studied both in the small and large cells. The product formation and nature was found to be different in these two cases although both were identical in the neat reaction. In the small cell there exists a competition between the recombination of CF_2 diradicals and oxidation, therefore, both C_2F_4 and COF_2 were observed. In the large cell, due to the relative overabundance of oxygen to the produced CF_2 and CHF_2 radicals (both large and small cells have the same irradiated volume), the final product was solely COF_2. However, CO and CO_2 were still not detected in either cell geometry. This

information further implies that CH radicals can not be formed at any reasonable concentrations since the oxidation of such CH radicals would produce CO(and/or CO_2). The failure to observe any CH and CHO bond containing compounds, thus, is in agreement with the products of the neat reaction of CH_2F_2 in the sense of production of the same primary radicals as summarized in equations (1) and (2).

In the study on the pyrolysis of polytetrafluoroethylene in oxygen, Kupel et al[7] have demonstrated that below 490°C carbonyl fluoride was the major product, and at higher temperatures further oxidation to CO_2 and CF_4 occurred. Mercury-Photo sensitized experiments[8] with C_2F_4-O_2 mixtures have also been found to produce COF_2 as the primary product and concluded that at room temperature CF_2 diradicals were unreactive toward oxygen. Therefore, from the observed products i.e., C_2F_4 and COF_2 in the small cell and COF_2 in the large cell, the processes seem to be controlled by physical configuration and composition of the reaction vessel instead of the temperature. The quenching effect in the high temperature reaction, which probably leads to different intermediate products, is then in essence controlled by diffusion of the excited species from reaction center to the cell wall.

(C) At a threshold pressure of 20 torr and a 1:1 ratio : The reactions were explosive. Explosions were found to be dependent on the reactants' ratio, pressure and the size and conditions of the reaction cell. The results are summarized below: (i) Explosions occurred at a 1:1 ratio of CH_2F_2 with O_2 mixture. No explosion was observed in the mixtrues of either CH_2F_2-rich or O_2-rich as (A) and (B) at the pressure ranges studied. (ii) At the total pressure of 20 torr, explosions were triggered by

the R(18)9.6μ laser line in a square cell (diameter, 4 cm; ratio of surface to volume, 0.83:1) as well as in a large cell (diameter, 10 cm; ratio of surface to volume, 0.60:1). In both cases green chemiluminescence was abundant. Under the same conditions, however, explosion was not triggerable in the small cell (diameter, 1.4 cm; ratio of surface to volume, 3.3:1). The results clearly indicate a non-thermal explosion limit with typical wall effects as the first explosion limit as is observed in the reaction of O_2 with H_2 at temperature around 550°C[15]. This effect of the size of the reaction cell is characteristic of chain termination at the wall since the time required for the chain propagators to diffuse to the wall increases with increasing diameter of the reaction cell. An additional experiment was performed in the square cell in which glass beads were added so as to change the area to volume ratio from 0.83:1 to 3:1. In this experiment the explosion was observed but with a different product distribution. Due to the physical situation of the glass beads, i.e., the bottom of the cell, the increase in the surface area does not effectively quench the explosion, however, it does show the wall effect on the product formation and results in a production of CO, CO_2 and COF_2. (iii) If the wall of the small cell was conditioned by using the old cell repeatedly without cleaning before each new experiment, the orange dominated emission of the explosion was also observed. In this case the wall could not effectively participate in terminating the chain since the glass was fluorinated as well as coated with fine carbon particulates left from the previous experiment. The observation of different emissions, corresponding to the different propagators that dominate the processes, does not change however the final product formation.

Identical results were found in the larger cell. (iv) Product formation was found to be dependent on the size of the reaction cell. COF_2 was observed in the small cell, CO and CO_2 were in the square cell and all three products were in evidence in the square cell after tripling its surface area with glass beads. Again, product formation was controlled by the size of the reaction cell. It must be pointed out that, in addition to the formation of SiF_4 in all cases, finely divided solid particulates were also observed in every explosion. No analysis was performed on the particulates although they are rather obviously carbon polymers. (v) A threshold pressure of 20 torr was required to induce an explosion when either the R(18)9.6μ or P(20)9.6μ laser lines were used as excitation sources. When the P(20)10.6μ line was used, the threshold pressure for the reaction to proceed identically must be increased to 40 torr in the square cell, however, no reaction at all was observed in the small cell even at 60 torr (i.e., 30 torr each). Since dielectric breakdown occurs at 25 torr (at 2J laser power) of pure CH_2F_2 in the small cell at this frequency, this unique observation might be explained by noting that there exists a high reaction cross-section of O_2 with thermal electrons.

7.4 Discussion

The energy transfer behavior of CH_2F_2 has been studied previously under low power excitation with the R(18)9.6μ laser line[6]. Qualitatively the V-V energy transfer scheme is very similar to CH_3F's behavior in that the C-F stretching vibrations are excited within 1 or 2 gas kinetic collisions at least to the v=3 of that ladder. Subsequently the excita-

tion transfers to the C-H stretching vibration at a lower rate in approximately 100 collisions. The V-T/R relaxation rate of the total manifold follows substantially slower at a rate of 45 $msec^{-1}torr^{-1}$. While this information is quite useful for the basic understanding of relaxation kinetics it becomes clear that a photon flux of some 10^{19} presents quite a different situation in terms of both the absorption efficiency and the subsequent inter and intramolecular V-V energy transfer rates. The low power excitation model would, for example, predict that the C-F vibrational ladder will be at a much higher vibrational temperature than the C-H ladder within the time regime of the laser pulse (.5 - 2μsec). Therefore one could legitimately doubt that reactions along the C-H coordinate would be catalyzed or induced at all. Yet, in the series of methyl halide reactions as well as in this work, essentially all products were uniquely those that proceeded along the C-H channel. The self consistency of the experimental results within this set of reactions as well as the increased efficiency of H atom removal to form radicals such as CHF_2 and CF_2 point toward a much more rapid excess energy deposition within the entire manifold and particularly in the C-H bond.

It is worth mentioning that a number of polyatomic dissociation reactions that have been studied previously all bear out the experimental observation that, when the molecular level density is high enough and the photon flux sufficiently high, unimolecular dissociation occurs in a time shorter than the laser pulse. Unfortunately little polyatomic energy transfer work whether V-V, E-V, or V-E has been reported on recently and yet it is precisely these data that are all important in predicting and understanding specific laser driven chemical

reactions.

The lack of such data does not however detract from the experimental observations that point clearly towards exceedingly rapid V-V equilibration times. Specifically we point out that in all methyl halides reactions and this work the major products formed invariably were those that were thermodynamically favored. In spite of the mode specific excitation, bond stability and thermodynamic considerations seem to dominate the chemistry that occurs subsequent to the laser pulse in these polyatomic species. Thus the mechanisms discussed below presuppose substantial V-V equilibration and possibly even V-E transfer and thus conform to the experimental observations.

Pyrolysis of CH_2F_2 has been studied by a jet method in the temperature range 750-1050°C[11]. It was suggested that decomposition of CH_2F_2 in the first stage into CHF and HF is responsible for the product formation of CH_2CF_2 and HF. However, CH_2CF_2 was not observed in this study as would be expected from such radical recombination, instead the copious formation of C_2F_4 implies the presence of the CF_2 radical. This difference would be attributed to the different reaction times inherent to these studies since product formation in the high temperature reaction strongly depends on the quenching rate. In addition, high pressure of N_2 which was added to dilute the reactant in a jet method can participate in the reaction since C_2, CH and CN are the most easily recognizable species can be found in the high temperature reaction[12].

Since C_2F_4 was not the only product formed in this reaction, processes other than the formation of CF_2 radicals must also exist. For example, production of C_2H_2 may be anticipated due to recombination of

such radicals as C_2, CH and H. Such recombination are likely to occur directly at the focal point of the entering beam since it represents the highest electron temperature. However, neither C_2F_4 nor C_2H_2 would be regarded as true final products of this reaction under the conditions used. Both C_2F_4 and C_2H_2 can be regarded as the intermediate products at fixed reaction times (order of 10^{-6} sec reaction time on each laser pulse for a preset number of laser pulses) and quenching rates (automatic quenching by the cell wall in a time period of excited species diffusion). Both intermediate products can be further decomposed during prolonged residence in the reaction zone (by increasing the number of laser pulses). Fig. 1 shows the results of this effect very clearly. (note: H_2O was not detectable due to adsorption by the NaCl windows, carbon was deposited over the whole wall area).

In the previous discussion the implication was made that two mechanisms operate in the two different pressure regimes and that CF_2 and CHF_2 radicals were present. The following mechanisms are suggested:

(a) $CH_2F_2 + n(h\nu) \rightarrow \cdot CHF_2 + \cdot H$ — High pressure regime >1 torr

$\cdot CHF_2 + Cl_2 \rightarrow CHF_2Cl + \cdot Cl$

$\cdot H + \cdot Cl \rightarrow HCl$

(b) $CH_2F_2 + n(h\nu) \rightarrow CH_2F_2^*$ — Low pressure regime <1 torr

$CH_2F_2^* + Cl_2 \rightarrow CH_2F_2 + 2Cl\cdot$

$CH_2F_2 + \cdot Cl \rightarrow CHF_2Cl + \cdot H$

$\cdot H + \cdot Cl \rightarrow HCl$

The latter mechanism is consistent with the observation that at low pressures the chlorine dependence is very critical. No dimerization reactions were discerned at pressures below one torr and therefore either mechanism (b) or the alternate (c) must predominate over the unimolecular

(c) $CH_2F_2 + n(h\nu) \rightarrow CH_2F_2^*$

$CH_2F_2^* + Cl_2 \rightarrow Cl_2 + \cdot CHF_2 + H\cdot$

$Cl_2 + H\cdot \rightarrow HCl + Cl\cdot$

$\cdot Cl + \cdot CHF_2 \rightarrow CHF_2Cl$

decomposition of CH_2F_2 at low pressures.

At pressures larger than one torr dimerization predominated in mixtures high in difluoromethane. Chlorine begins to compete efficiently at 1:1 ratios at pressures higher than 5 torr in large vessels (500 c.c.). In the smaller 18 c.c. cells chlorine begins to compete efficiently at ratios of 4:1 and total mixture pressures of 10 torr. The observed products however are, as was noted earlier, independent of reactant pressures. Thus mechanism (a) in which either CH_2F_2 or Cl_2 compete for the created radical is definitely favored. The reduced stability of the C-H bond relative to CH_3F argues favorably for this mechanism as well.

As in all free radical reactions, dependence is noted on cell wall proximity and relative size. Smaller cells (i.e., closer walls) favor the dimerization reactions and higher yields of SiF_4 while larger cells yield lesser dimers and higher concentrations of the chlorinated species (CHF_2Cl or CF_2Cl_2). This behavior is of course confined to the higher pressure regime. No such dependence was noted at pressures below

one torr where only the chlorinated product predominated.

In the reactions of CH_2F_2 with Cl_2 it was found that the final products were the di-chlorinated species. No trichlorinated or totally chlorinated products were detected as the result in the thermodynamically favorable in C-F bond over C-Cl bond. In the oxidation reaction of CH_2F_2, the fully oxidized products were also found presumably due to the same effect namely that the C=O bond is favored over the C-F bond in glass systems. However, this substitution was controlled by the size of the reaction cells. As shown in Table 3, neither CO_2 nor CO were observed in the small cell even at high ratios of oxygen, formation of C_2F_4 still competes with that of COF_2 at a 1:1 ratio at low pressure in the small cell. On the other hand, C_2F_4 was not found in the large cell even at high ratios of CH_2F_2. Therefore, the size of the cell was the determining factor for the final product formation. Since the irradiation volume was maintained constant, the only difference between the reaction proceeding in the large cell (CH_2F_2:O_2 = 5:1, at 9 torr) and in the small cell (CH_2F_2:O = 1:1, at 12 torr) was the distance between the reaction center to the cell wall (4.9 cm and 0.7 cm,respectively). The excited species experiences many more collisions before reaching the wall in the large cell. Thus, formation of C_2F_4 is clearly aided by wall recombinative processes and is clearly quenched by increased number of collisions. The wall effects are even more obvious in the explosive reaction. The cell walls are effective for deactivation and especially so for removing the excess released energy by the recombination process. If the walls are new, they do not contribute appreciably to recombination. However, if the walls are "dirty", the recombination process often occurs with

very high rates. Both observations relating to the explosive reactions are thus acceptable on these grounds: the formation of polymers and the ease of explosive ignition in small "dirty" cells.

The explosions only occur at a 1:1 rato of CH_2F_2 to O_2 with a total threshold pressure of 20 torr in either a clean large cell or a coated small cell, when either R(18)9.6μ or P(20) 9.6μ were used as excitation sources. If P(20)10.6μ laser line was used the threshold pressure had to be increased significantly in order to obtain the same product. From the product formation, COF_2 found in the small cell and CO and CO_2 found in the large one, it is clear that the laser served only as an initiator for the explosive reaction and the chemistry following the explsoion was independent of the excitation source. No detailed measurements on the threshold laser power were made, but, as the power was reduced, it was found that the explosion could be triggered after a few tens of laser pulses. This may be due to the necessity of "preparing" the walls to induce the explosion at such a low laser power. The electronic emission following the explosion showed different colors from the one occurred in a clean cell. The difference of the colors, green in a clean walls and orange in a coated walls, is attributed to the different concentration of propagators produced during the course of the explosion due to the degree of participation from the walls.

It was attempted to ignite the explosive reaction of H_2 with O_2 at 2:1 ratio at 40 torr (the threshold presoure for explosive reaction of CH_2F_2 with O_2 when irradiated off-resonantly), however, no explosion occurred. At 150 torr of total and 2:1 ratio the orange explosion was observed in the reaction of H_2 with O_2 but the explosive power was much

lower than that of observed with CH_2F_2 and O_2. At 100 torr, the explosion of the CH_2F_2-O_2 mixtures prepelled the NaCl windows of the irradiation cell, a few meters away and particles of the polymer (teflon) were clearly observed all over the cell wall.

The mechanism for this CH_2F_2 reaction with and without presence of O_2 is suggested which accounts for all of these observations:

$$CH_2F_2 \xrightarrow{nh\nu} CHF_2 + H \qquad (1)$$

$$CHF_2 \longrightarrow CF_2 + H \qquad (2)$$

$$CHF_2 + O_2 \longrightarrow COF_2 + OH \qquad (4)$$

$$CF_2 + CF_2 \xrightarrow{wall} C_2F_4 \qquad (7)$$

$$CF_2 + O_2 \xrightarrow{wall} COF_2 + O \qquad (5)$$

$$H + O_2 \longrightarrow OH + O \qquad (8)$$

$$COF_2 + O \longrightarrow CO_2 + F_2 \text{ (or } CO + OF_2) \qquad (9)$$

$$H + OH \longrightarrow H_2O \qquad (10)$$

$$O + OH \xrightarrow{wall} O_2H \qquad (11)$$

Equatious (1), (2) and (7) are responsible for the formation of C_2F_4 in the neat reaction of CH_2F_2. For the reactions in excess of O_2 equations (4) and (5) are important and equation (7) is negligible. In the CH_2F_2-rich reactions, however, equations (4), (5) and (7) are equally important so that there were existed both COF_2 and C_2F_4. In the large cell, a further oxidation of COF_2 occurred such that equation (9) proceeded towards formation of CO and CO_2. In an explosive chain reaction, H produced from both equations (1) and (2) is considered to be an initial propagator. The propagation progress includes equations (4), (5) and (8) in which only step (8) involves chain branching. The termination steps are (7), (9), (10) and (11). The large rate increase during the branched explosion can easily account for the polymerization of CF_2 and the

observation of a powerful shock wave as discussed earlier.

7.5 Conclusions

The observation summarized in this chapter are consistent with previous work both performed in our laboratory and eleswhere. Although low power energy transfer information "predicts" a more highly reactive C-F channel the C-H channel is favored almost exclusively as the products are thermodynamically preferred. The existence of a unimolecular mechanism for decomposition of CH_2F_2 prior to its reaction with Cl_2 at pressures above one torr is shown as is a collisionally controlled mechanism at lower pressures. The reaction efficiency is quite high and at higher pressure proceeds appreciably with one laser shot of a 1 Joule energy content. The products, however, unless removed continue to react aided by either existing laser overlaps or via collisional transfer from high lying states in CH_2F_2.

Explosion was ignited for a reaction of a 1:1 reatio of CH_2F_2 to O_2 at threshold pressure of 20 torr by a CO_2 TEA laser. The electronic emission following the explosion displayed different colors corresponding to the predominance of different chain propagators. Products of this reaction can be controlled by using different size cells. With a small cell, the reactive species experience less collisions. In a larger cell (500 cm^3 volume) many more collisions are experienced by the reactive fragments before wall quenching is effective. Thus it would be expected that in the smaller cell the primary oxidation product, COF_2 should predominate while the final oxidation products CO and CO_2 should

be in greater abundance in the larger cell. Experimental results verified these expectations thus pointing out the importance of gas-solid quenching rate in laser induced reactions. An additional piece of evidence supporting wall participation is the experimental findings of polymeric material uniformly distributed over the cell walls. In significant concentrations, such as in the large volume cell, these polymers are easily identifiable by eye.

References

1. A. M. Ronn, Spectry Letters, 8, 303 (1975).

2. J. T. Knudtson and E. M. Eyring, Ann. Rev. Phys. Phys. Chem. 24, 255 (1974).

3. N. G. Basov, A. N. Oraevsky, and A. V. Pankratov, in: Chemical and Biochemical Applications of Lasers, C. B. Moore, Ed., Academic Press, New York, 1974.

4. A. L. Robinson, Science 193, 1230 (1976).

5. B. L. Earl and A. M. Ronn, Chem. Phys. Letters 41, 29 (1976).

6. L. A. Gamss and A. M. Ronn, Chem. Phys. 9, 319 (1975).

7. R. E. Kupel, M. Nolan, R. G. Keenan, M. Hite and L.D. Scheel, Anal. Chem. 36, 386 (1964).

8. J. Heicklen, V. Knight and S. A. Greene, J. Chem. Phys. 42, 221 (1965).

9. M. Venugopalan, Ed., Reactions Under Plasma Conditions, Vol. II, Wiley-Interscience, New York, 1971.

10. N. R. Isenor and M. C. Richardson, Appl. Phys Lett. 18, 224 (1971).

11. S. F. Politanskii and V. U. Shevchuk, Kinetika i Kataliz 8, 12 (1967); 9, 496 (1968).

12. G. M. Burnett and A.M. North, Transfer and Storage of Energy by Molecules, Vol. I, Electronic Energy, Wiley-Interscience,New York, 1969.

13. J. L. Frankin, J. G. Dillard, H. M. Rosenstock, J. T. Herron, K. Draxl and F. H. Field, Ionization Potentials, Appearance Potentials, and Heats of Formation of Gaseous Positive Ions, NSRDS-NBS 26, Office of Standard Reference Data, National Bureau of Standards, U. S. Department of Commerce, Washington, D. C. (1969).

14. E. K. Plyler and W. S. Benedict, J. Research NBS 47, 202 (1951).

15. S. W. Benson, Foundations of Chemical Kinetics, McGraw-Hill Book Company, New York, 1960.

16. J. R. Nielsen, H. H. Claassen and D. C. Smith, J. Chem. Phys. 18, 812 (1950).

Figure 1 Caption

Successive infrared spectra of CH_2F_2 taken at 10 torr pressure[14]. Arrow denotes location of C_2F_4 peak[16]. SiF_4 peak's growth is evident at 1030 cm^{-1}. All other peaks are parent peaks of CH_2F_2. In the five spectra the number of laser shots is indicated on the left.

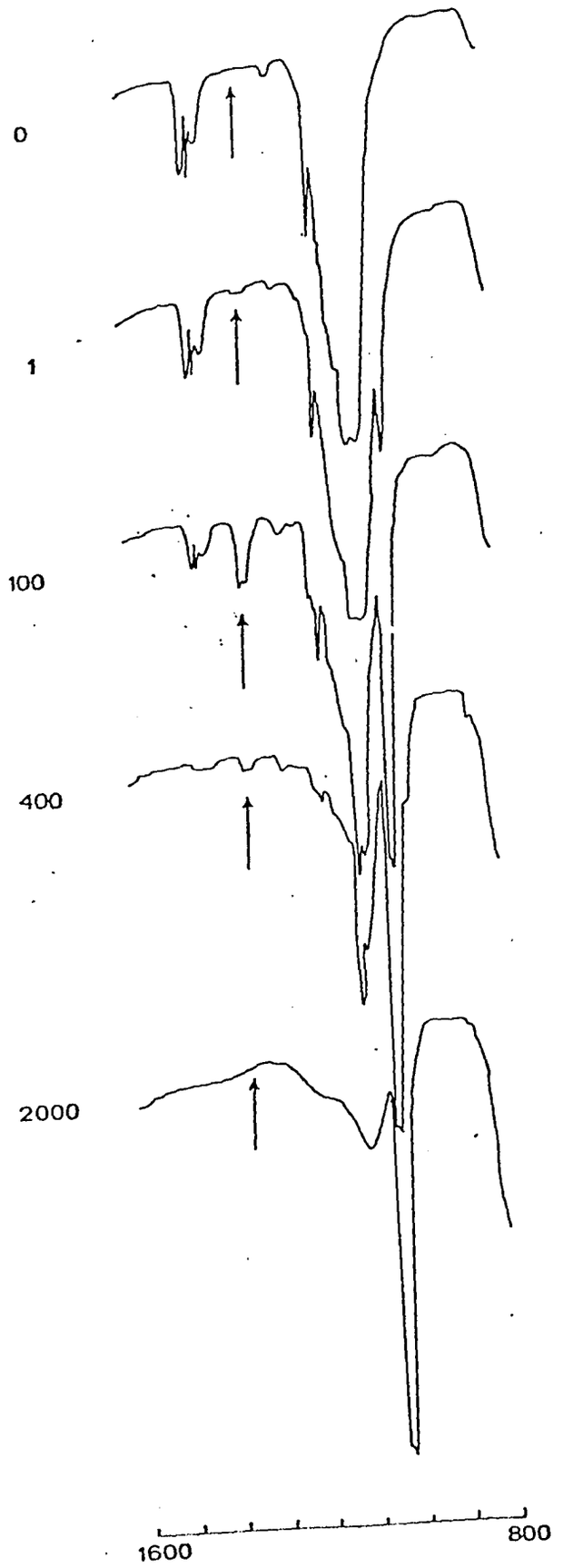

Figure 1

Chapter 8

REACTIONS OF FLUOROMETHANES INDUCED BY INFRA-RED LASER BREAKDOWN

8.1 Introduction

A chemical reaction can be induced by an intense infrared laser radiation either through multiphoton absorption processes or gas breakdown. By multiphoton absorption processes the investigated molecules have to possess a particular vibrational frequency. Molecules which have no vibrational frequency between 9.2 to 11 μ are thus not available for study by this method. However, these molecules can be studied by the process of laser induced gas breakdown. This process normally attributable to the very high AC electric field generated by the intense infrared radiation is usually circumvented in isotope separation experiments by carefully varying gas pressures and irradiation intensities. The reaction that proceeds under plasma (spark) conditions by means of dielectric breakdown is thus related to conventional high temperature chemical studies.

There are a number of obvious merits to the use of such a process to induce chemical reactions. Undoubtedly, the potential use of this high efficient method is to combine it with the selective multiphoton absorption technique as a hybrid system which would be expected to be able to benfit from both strong points while circumventing each deficiency to some extent. It is a very clean system as opposed to conventional high temperature reaction. It is not necessary to have high

pressure of carrier gas since reactions can be induced at pressures from a few torr and up depending on the characteristics of sample molecules under particular laser conditions. With higher laser fluence the threshold pressure can further be reduced. Therefore, no perturbation of the system from foreign gases needs to be accounted for. Reactions under high temperature conditions usually require quenching partners however the laser induced reaction is automatically quenched at pulse termination and scavenging is not necessary. Since the reaction times using this method are very short, generally within a few microsecond the cell wall servs as an automatic quenching system, the rate can be controlled by varying the distance between the reaction center and cell wall(due to the diffusion of the excited species onto the wall). By choosing the cell materials, the cell can become a scavenger and inhibit recombination steps. The temperature generated in this method is high from 1 to 10 eV in various gases[1] and in fact electrons generated from inside core of the plasma were found carried the energy as high as 10 KeV.[2]

The series of possible reactions in CH_4, CH_3F, CH_2F_2 and CHF_3 were studied using the LIDB technique. Of importance were the comparative homologous results for threshold pressure, efficiency and product distribution. Thses results are discussed and compared with available pyrolysis data[3] on the same series.

8.2 Experimental

The laser apparatus was essentially the same as that used in Chapter 5. Regular infrared gas glass cells with a volume of 18 cm^3 were used.

A 5 inch focal length ZnSe lens was used to increase the fluence of the laser by as much as 100-fold. Laser conditions were preset and carefully matched for all experiments. The laser frequency was set at P(20) 10.6μ line guaranteeing that none of the studied gases show a matched vibrational frequency and a possible absorption. This precaution was taken so as to avoid multiphoton absorption processes for all measurements. The laser output was carefully maintained at 2J and the results were analyzed by infrared spectroscopy after 50 laser pulses. Gas pressure was carefully varied until consecutive 50 plasma sparks were observed for 50 input pulses. This pressure then corresponds to the true threshold pressure of the measured gas. The repetition rate was fixed at 50 pulses per minute, i.e., one experiment was finished in one minute. The low number of laser pulses is inherent to the LIDB technique's efficiency. As can be seen from Table 1, CH_2F_2 showed 50% decomposition in 50 pulses. With a low number of laser pulses, the products were easily measurable and further decomposition of the products can thus be avoided.

Sample gases of CH_4, CH_3F and CH_2F_2 were Matheson research grade and used without further purification save for freeze thaw cycles. Fluoroform obtained from prof. Ishida's laboratory was laboratory grade with minimum purity of 98%. No further purification was made, however, since no impurities were found from preexperimental infrared spectra.

The percent decomposition of parent molecules and C_2H_2 production were calculated by monitoring the reduction of parent peaks and the formation of C_2H_2 peaks of infrared spectra prior to and subsequent to the laser radiation. Infared spectra were taken at slow scan rate

TABLE 1

Results obtained from nonresonant laser induced breakdown

Reactant	Threshold pressure (torr)	% decomposition after 50 pulses	Quantum yield (molcules decomposed per photon used)	Products	C_2H_2 produced (torr)
CH_4	60	8.3	5.6×10^{-4}	C_2H_2	2.5
CH_3F	50	24.	1.3×10^{-3}	Carbon, C_2H_2, SiF_4	5.0
CH_2F_2	25	48.	1.3×10^{-3}	Carbon, C_2H_2, SiF_4 C_2F_4	1.0
CHF_3	45	22.	1.1×10^{-3}	Carbon, SiF_4, C_2F_6 C_2F_4, CF_4, COF_2 (trace)	—

with a perkin-Elmer Model 267. The products were identified by comparison of infrared spectra with the standard charts. Since all products and reactants have very distinct absorption peaks in infrared spectra, identification of products is easily accomplished. The characteristic peaks of products in cm^{-1} are: C_2H_2, 3310 and 730; SiF_4, 1030; C_2F_4, 1332 and 1342; CF_4, 1283; C_2F_6, 1250 and 1117; COF_2, 1926, 1942 and 1957.

To calculate the number of photons and sample molecules, the ideal gas law was used without correction. One joule of laser energy at 944.15 cm^{-1} calculates out as equal to 5.3×10^{19} photons and one torr of sample in a 18 cm^3 cell equals to 5.8×10^{17} molecules. The quantum yield is defined as the number of molecules decomposed per photon used. The results are shown in Table 1.

8.3 Results

Table 1 shows the threshold pressure, percent decomposition, pressure of C_2H_2 produced, quantum yield and product formation for all four gases. The threshold pressure for different gases at identical laser conditions is expected to show a dependence on the nature of gases in this experimental process. In order to correlate the results with the molecular properties of the studied gases, a list of thermodynamic data is shown in Table 2.

To induce a breakdown at a fixed laser condition, it is expected intuitively that threshold pressure should increase with increasing ionization potential and with decreasing dipole moment and polarizability in a strong electric field. However, gas breakdown induced by a CO_2

TABLE 2

Thermodynamic properties of fluorinated methanes

Molecule	Dissociation Energy[a] (Kcal/mole) C-H	C-F	Ionization potential[b] to remove H atom (eV)	Dipole[c] moment, μ (Debye)	Polarizability[d], α ($\AA^3$)	Induced[f] dipole moment, αE (Debye)
CH_4	104.0	——	14.3	0	2.62	0.048
CH_3F	103.1	108.6	14.0	1.85	2.62	0.048
CH_2F_2	101.0	121.9	13.1	1.97	2.72[e]	0.050
CHF_3	106.2	125.8	14.0	1.65	2.81	0.051

a. R.J. Blint, T. B. McMahon and J.L. Beauchamp, J. Am. Chem. Soc. 96, 1269 (1974).

b. National Bureau of Standards, NSRDS-NBS 26, issued 1969.

c. ibid, NSRDS-NBS 10, issued 1967.

d. J. Applequist, J. R. Carl and K.K. Fung, J. Am. Chem. Soc. 94, 2952 (1972).

e. Estimated.

f. $E = 5.5 \times 10^6$ V/cm

laser favors avalanche ionization, as mentioned in Chapter 4, so that production of electrons and ions are the primary processes. Therefore, only the ionization potential of gases would be the direct parameter to affect this process. The induced dipole moment, the product of polarizability and field intensity, is usually much smaller than the permanent dipole moment as shown in the Table 2. There appears to be no obvious correlation between threshold pressure and induced dipole or permanent dipole or both. This would be the case if the threshold pressure is determined by the early stages of breakdown where production of either initial or free electrons is the most important factor. Thus ionization potential is the only important parameter directly related to this stage. There also appears no obvious linkage to the bond strength of molecules,i.e., radical formation in the early stages of breakdown. Fig. 1 shows the plot of threshold pressure against ionization potential of all four gases. The results show that the threshold pressure is proportional to the ionization potential of the gases. The higher the ionization potential of the gas, the higher the threshold pressure of the gas.

The results in percent decomposition show that CH_2F_2 is the highest in this series, CH_3F and CHF_3 about the same and CH_4 is the lowest. The quantum yields show that CH_3F, CH_2F_2 and CHF_3 have approximately the same value whereas CH_4 is only half as large. The following considerations expand somewhat of the implications of these observations. The laser energy applied to the system is charaterized by plasma formation, Chemical processes on the other hand occur mostly outside the plasma. Due to the very similar values of the weakest C-H bond strengths,

the moleoules' decomposition seems to depend only on the available energy, i.e., the available number of photons. For example, the original numbers of CH_2F_2 molecules are the lowest among all four gases so that the percent decomposition is the highest. The fact that CH_4 showed a reduced quantum yield is most likely due to efficient radicals recombination of H + CH_3 to reform CH_4. Further evidence of this recombination is failure to observe solid carbon particulates during the reaction (our experimental conditions can detect over a minimum size of 60 Å). The glass cells also affect the difference of quantum yields between fluorinated methanes and methane. Glass functions as an efficient scavenger for fluorinated species due to formation of the stable compounds SiF_4 and H_2O, thus recombination processes in CH_3F, CH_2F_2 and CHF_3 have only very low probability of occurrence.

$$4HF + SiO\ (glass) \longrightarrow SiF_4 + 2H_2O$$

The failure to observe C_2H_2 in the case of CHF_3 dissociation supports this hypothesis rather well.

The only product observed in the decomposition of methane is C_2H_2. This is the only high temperature species that is also found at ambient temperature. From thermodynamic data, the free energy of formation shows that only the paraffinic hydrocarbons are thermodynamically stable below 500°K; olefins and acetylenes are all unstable. Especially, acetylene is unusual in having a free energy of formation that decreases with increasing temperature. The data also show that acetylene is the most stable compound above 1500°K[4]. At ~1400°K both CH_4 and C_2H_2 have equally thermodynamic stability and below this temperature CH_4 is more stable than C_2H_2. Since C_2H_2 becomes relatively

unstable the reaction core is cooled it follows that in order to obtain a high yield of acetylene a rapid method of quenching has to be provided. Based on the experimental observations of C_2, CH species as dominant in high temperature reactions of C/H containing compounds (in addition to large abundant of H atom) the following reactions may well account for the product formation observed here and in other studies:

$$C_2 + H \longrightarrow C_2H$$
$$CH + CH \longrightarrow C_2H_2$$
$$C_2H + H \longrightarrow C_2H_2$$
$$C + 4H \longrightarrow CH_4$$

The C_2 and C in the vapor phase do not aggregate to form solid pacticulates since a high excess of atomic hydrogen(Formation of carbon with size smaller than 60 Å can not be observed here).

Since the formation of acetylene is favored by increasing the C/H ratio at constant temperature, the increased amounts of C_2H_2 found in the CH_3F raction as opposed to the CH_2F_2 and CF_3H are clearly aided by the glass wall scavenging of F and HF fragments. The lower concentration of hydrogen atoms in this reaction also led to deposit of carbon particulates since the latter aggregate more easily from the vapor phase.

In the reaction of CH_2F_2 the formation of CF_2 and possibly C_2F_2 which competed with C_2 and CH resulted in the reduction of C_2H_2 and increasing in the formation of C_2F_4 (The C_2F_2 is never found at room temperature if it were formed during the reaction the final products should be either C_2F_4 or carbon).

C_2H_2 was not observed in the reaction of CHF_3 thus ruling production of the CH radical formation as unlikely. The formation of CF_3, CF_2 and C_2F_2 radicals can account for the formation of all the observed products. A large amount of SiF_4 formation may also lead to the observable quantity of COF_2. The reactions may be summarized as following

$$2CF_2 \longrightarrow C_2F_4$$
$$2CF_3 \longrightarrow C_2F_6$$
$$C_2F_2 + 2F \longrightarrow C_2F_4$$
$$CF_3 + F \longrightarrow CF_4$$
$$F + SiO_2 \text{ (glass)} \longrightarrow SiF_4 + 2O$$
$$CF_2 + O \rightarrow COF_2$$
$$C_2(g) \longrightarrow 2C(s)$$
$$C_2 + 8F \longrightarrow 2CF_4$$

8.4 Discussion

The properties of a molecule most affected by a strong oscillating AC field are the dipole moment and induced dipole moment which together constitute the total polarization. Depending on the frequency, the total polarization can be described as orientation, atomic and electronic polarization. At a frequency of 10^{13} sec^{-1} (laser frequency) the most significant part of the total polarization is the atomic polarization, i.e., the distortion between positive and negative atoms. Therefore, the ionization potential of removing an atom and an electron from the

parent molecule is thought to be the most closely related parameter to the threshold pressure. This can be seen from the proposed mechanism of avalanche ionization for inducing an optical breakdown in a laser field. A chain production of electrons and ions determines this process. To determine this relationship of ionization potential to other factors responsible for breakdown, however, for one gas in not possible since the ionization potential is a fixed constant as shown in Chapter 4 equation (3).

From Chapter 4 equation (3), the power density required for breakdown is given as

$$(P/A) = \frac{2\, m_e \epsilon\, c\, I_p\, \nu^2 \ln(n_e/n_o)}{e^2\, \nu_e\, \tau}$$

One can rearrange this equation

$$\nu_e = \frac{2\, m_e \epsilon\, c\, I_p\, \nu^2 \ln(n_e/n_o)}{e^2\, \tau\, (P/A)}$$

For a fixed laser power density, the electron-molecule collision frequency ν_e becomes the threshold condition to induce a breakdown. Since ν_e is directly proportional to the pressure of the molecule, this equation can be rewritten as

$$P = k\, \nu_e = k'\, I_p$$

where k and k' are the proportionality constants. This is to say that, for a fixed laser power density, the threshold pressure is directly proportional to the ionization potential of the molecule. This relation is readily applicable to study the correlation between the threshold pressures for different molecules, which have different ionization potentials, and identical laser fluence conditions. Indeed, as shown in Fig. 1, this correlation is fairly good in this series of molecules.

Laser induced chemical reactions under plasma conditions belong to the high temperature category and thus thermodynamically controlled. The plasma can be differentiated into two regions, the small dense core dominated by ionic species and the less dense region dominated by free radicals and atoms. Ions have very short life times so that chemical processes occurring in this region could be ignored. For the high pressures used throughout this study, most chemistry would be expected to proceed outside this dense core and may well include the cell wall as part of a gas-solid reaction. This is supported by the results obtained from the reaction of CH_2F_2 which had the highest percent decomposition with the lowest initial reaction pressure.

The cold gas molecules surrounding the outside of the plasma are not only behaving as quenching agents but also prevent the free movement of the highly excited species produced inside the plasma and gaining the energy either from collisions or from the released energy due to association of the radicals. These processes operate so rapidly, efficiently and result in little if any translational temperature changes in the bulk. The exclusive and high product yield of C_2H_2 in the reactions of CH_4 and CH_3F provide evidence in support of exceedingly

high quenching rate.

It is perhaps worthwhile to mention at this point that laser induced chemical reactions of almost any hydrocarbons always show C_2H_2 as a major product and eventually the exclusive product as the irradiation continues. As mentioned previously, this result is attributed to the conditions of the high temperature and fast quenching rate. This indicates that the characteristics of the laser induced chemical reactions through gas breakdown is short reaction time, high temperature and rapid, automatic quenching.

A general scheme for the pyrolysis of the fluoromethanes was proposed subsequent to a study involving the jet method in the temperature range 750-1050°C.[3] The scheme is as follows

$$RHF \longrightarrow R + HF$$

$$RHF + R \longrightarrow R{=}R + HF$$

$$R{=}R + R \longrightarrow \text{addition products}$$

$$R + R \longrightarrow R{=}R$$

$$R{=}R \longrightarrow \text{decomposition products}$$

where R= CH_2, CHF or CF_2. However, this scheme can not be used to interprete the product formation obtained from this study. Although, experiments by both methods were at high temperature and show thermodynamically controlled production, there exist intrinsic differences in the experimental methods themselves as discussed in Chapter 7. The proposed mechanisms above were mainly attributed to the decomposition of the reactant molecules, however, at high temperature only atomic

species and fragments which have the lowest free energy are stable and product formation is mostly due to the recombination of fragments and atoms under the influence of the quenching rate.

Finally, one point has to be emphasized that the product formation of laser induced reactions either by multiphoton absorption processes or via gas breakdown always show the same results. So far reactions of SF_6, CH_2F_2, CH_3F, CrO_2Cl_2 and OCS with or without scavengers such as H_2, O_2 and Cl_2 have been examined here. Additionally, at least twenty other systems were studied elsewhere. To explain both processes via the same mechanism is attractive since some very suggestive clues imply that the multiphoton absorption process is also probably a high temperature, thermodynamically controlled mechanism. Clues such as (i) Existence of C_2 and CH were identified from laser induced luminescence through multiphoton absorption process[5]. (ii) NH_2 radical was observed after NH_3 was irradiated with 60 different laser lines either on or off resonance[6]. (iii) The statistical thermodynamic rate equation can be applied to the incoherent region in the collisionless multiphoton dissociation processes[7]. The incoherent region is quasi-continuum states far below the dissociation limit. (iv) The fact that identical final products have been observed in a very large number of studies of on and off resonant excitation is by far the most suggestive. These are summarized in the conclusions to follow.

8.5 Conclusions

Laser induced gas breakdown was applied to the series CH_4, CH_3F,

CH_2F_2 and CHF_3. The threshold pressures of individual gases in this series were found to be directly proportional to the ionization potentials of the respective gases. The applicability to the equation proposed by avalanche ionization mechanism provides evidence that a moderate power CO_2 laser with pulse duration of ~1 μs favors the mechanism for LIDB (laser induced dielectric breakdown). The highest percent decomposition of the CH_2F_2 reaction with its lowest initial pressure implies that the major chemical processes occur outside the small dense core and essentially isotropically throughout the whole reaction cell. The same quantum yield obtained for CH_3F, CH_2F_2 and CHF_3 implies that plasma formation is only a primary step and that the controlling chemistry occurs as a secondary process that depends on the total available energy. The peculiarity of producing C_2H_2 as a major product in laser induced reactions of hydrocarbons and of molecules with higher numbers of C and H atoms through breakdown suggests that the characteristics of the reactions agree well with the model predicted on short reaction time, high temperature and rapid, automatic quenching.

References

1. M. Venugopalan, Reactions Under Plasma Conditions, Vol. II, M. Venugopalan, Ed., Wiley-Interscience, New York, 1971.

2. E. Yablonovitch, Phys. Rev. Lett. 35, 1346 (1975).

3. S. F. Politanskii and V. U. Shevchuk, Kinetika i Kataliz 8, 12 (1967); 9, 496 (1968).

4. J. T. Clarke, The Application of Plasmas to Chemical Processing, R. F. Baddour and R. S. Timmins, Eds., The M. I. T. Press, Cambridge, Mass., 1967.

5. N. R. Isenor and M. C. Richardson, Appl. Phys. Lett. 18, 224 (1971)

6. J. D. Campbell, G. Hancock, J. B. Halpern and K. H. Welge, Chem. Phys. Lett. 44, 404 (1976).

7. J. G. Black, E. Yablonovitch, N. Bloembergen and S. Mukamel, Phys. Rev. Lett. 38, 1131 (1977).

Figure 1 Caption

The dependence of the threshold pressure on the ionization potential of a series of molecules CH_4, CH_3F, CH_2F_2 and CHF_3. The laser conditions used in this study were at the power energy of 2J and the pulse duration of ~1 μs.

Figure 1

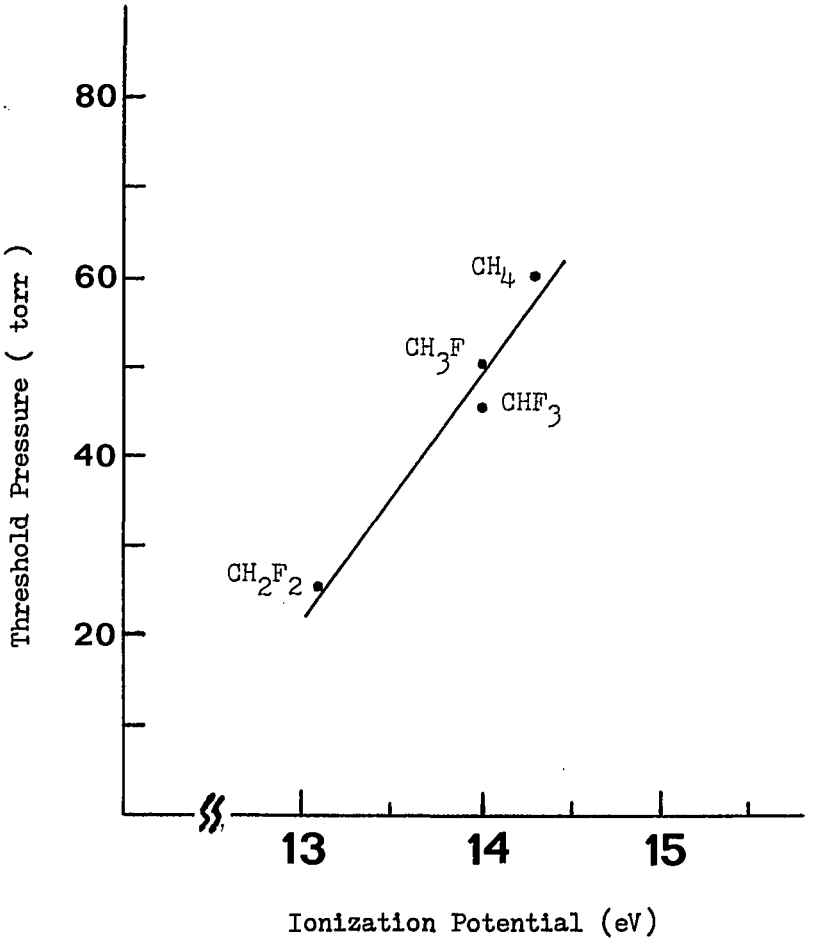
80
60
40
20
Threshold Pressure (torr)
CH_4
CH_3F
CHF_3
CH_2F_2
13
14
15
Ionization Potential (eV)